ARMY RESEARCH LABORATORY

A Multiscale Gradient Theory for Single Crystalline Elastoviscoplasticity

by John D. Clayton, David L. McDowell, and Douglas J. Bammann

ARL-RP-117 **February 2006**

A reprint from the *International Journal of Engineering Science*, vol. 42, pp. 427–457, 2004.

NOTICES

Disclaimers

The findings in this report are not to be construed as an official Department of the Army position unless so designated by other authorized documents.

Citation of manufacturer's or trade names does not constitute an official endorsement or approval of the use thereof.

Destroy this report when it is no longer needed. Do not return it to the originator.

Army Research Laboratory
Aberdeen Proving Ground, MD 21005-5066

ARL-RP-117 **February 2006**

A Multiscale Gradient Theory for Single Crystalline Elastoviscoplasticity

John D. Clayton
Weapons and Materials Research Directorate, ARL

David L. McDowell
Georgia Institute of Technology

Douglas J. Bammann
Sandia National Laboratories

A reprint from the *International Journal of Engineering Science*, vol. 42, pp. 427–457, 2004.

REPORT DOCUMENTATION PAGE

Form Approved
OMB No. 0704-0188

1. REPORT DATE *(DD-MM-YYYY)*	2. REPORT TYPE	3. DATES COVERED (From - To)
February 2006	Reprint	1 January 2003–1 January 2006

4. TITLE AND SUBTITLE
A Multiscale Gradient Theory for Single Crystalline Elastoviscoplasticity

5a. CONTRACT NUMBER

5b. GRANT NUMBER

5c. PROGRAM ELEMENT NUMBER

6. AUTHOR(S)
John D. Clayton, David L. McDowell,[*] and Douglas J. Bammann[†]

5d. PROJECT NUMBER
1L1622618AH80

5e. TASK NUMBER

5f. WORK UNIT NUMBER

7. PERFORMING ORGANIZATION NAME(S) AND ADDRESS(ES)
U.S. Army Research Laboratory
ATTN: AMSRD-ARL-WM-TD
Aberdeen Proving Ground, MD 21005-5066

8. PERFORMING ORGANIZATION REPORT NUMBER
ARL-RP-117

9. SPONSORING/MONITORING AGENCY NAME(S) AND ADDRESS(ES)

10. SPONSOR/MONITOR'S ACRONYM(S)

11. SPONSOR/MONITOR'S REPORT NUMBER(S)

12. DISTRIBUTION/AVAILABILITY STATEMENT
Approved for public release; distribution is unlimited.

13. SUPPLEMENTARY NOTES
A reprint from the *International Journal of Engineering Science*, vol. 42, pp. 427–457, 2004.
[*]George W. Woodruff School of Mechanical Engineering, Georgia Institute of Technology, Atlanta, GA 30332-0405.
[†]Department of Science-based Materials Modeling, Sandia National Laboratories, Livermore, CA 94551.

14. ABSTRACT
Explicit volume averaging procedures are used to motivate a gradient-type description of single crystalline elastoviscoplasticity. Upon regarding local elastic and plastic deformation gradients within the crystal as continuously differentiable fields, we arrive at a three-term multiplicative decomposition for the volume-averaged deformation gradient, consisting of a recoverable elastic term associated with the average applied stress and average lattice rotation, an inelastic term associated with the average plastic velocity gradient, and a (new) third term reflecting the presence of the residual microelastic deformation gradient within the volume and providing a representation of the kinematics of grain subdivision via formation of low-angle subgrain boundaries, for example. A variant of the classical Eshelby stress tensor provides the driving force for homogenized viscoplastic flow, with slip resistances dictated by densities of geometrically necessary and statistically stored dislocations. Distinctive features of the continuum model include coupling of internal elastic strain energy densities associated with residual and applied stresses, dependency of the single crystalline effective elastic moduli upon evolution of lattice substructure, and a characteristic length potentially based upon both the size of the crystal element used in volume averaging and the grain subdivision measure.

15. SUBJECT TERMS
crystal plasticity, dislocations, disclinations, lattice defects, multiscale models

16. SECURITY CLASSIFICATION OF:			17. LIMITATION OF ABSTRACT	18. NUMBER OF PAGES	19a. NAME OF RESPONSIBLE PERSON
a. REPORT	b. ABSTRACT	c. THIS PAGE			John D. Clayton
UNCLASSIFIED	UNCLASSIFIED	UNCLASSIFIED	UL	38	19b. TELEPHONE NUMBER (*Include area code*) (410) 306-0975

Available online at www.sciencedirect.com
SCIENCE DIRECT®
ELSEVIER
International Journal of Engineering Science 42 (2004) 427–457
International Journal of Engineering Science
www.elsevier.com/locate/ijengsci

A multiscale gradient theory for single crystalline elastoviscoplasticity

J.D. Clayton [a], D.L. McDowell [b,*], D.J. Bammann [c]

[a] *Impact Physics Branch, US Army Research Laboratory, Aberdeen Proving Ground, MD 21005, USA*
[b] *George W. Woodruff School of Mechanical Engineering, Georgia Institute of Technology, Atlanta, GA 30332-0405, USA*
[c] *Department of Science-based Materials Modeling, Sandia National Laboratories, Livermore, CA 94551, USA*

Received 25 August 2003; accepted 25 August 2003

(Communicated by JOHN W. HUTCHINSON)

Abstract

Explicit volume averaging procedures are used to motivate a gradient-type description of single crystalline elastoviscoplasticity. Upon regarding local elastic and plastic deformation gradients within the crystal as continuously differentiable fields, we arrive at a three-term multiplicative decomposition for the volume-averaged deformation gradient, consisting of a recoverable elastic term associated with the average applied stress and average lattice rotation, an inelastic term associated with the average plastic velocity gradient, and a (new) third term reflecting the presence of the residual microelastic deformation gradient within the volume and providing a representation of the kinematics of grain subdivision via formation of low-angle subgrain boundaries, for example. A variant of the classical Eshelby stress tensor provides the driving force for homogenized viscoplastic flow, with slip resistances dictated by densities of geometrically necessary and statistically stored dislocations. Distinctive features of the continuum model include coupling of internal elastic strain energy densities associated with residual and applied stresses, dependency of the single crystalline effective elastic moduli upon evolution of lattice substructure, and a characteristic length potentially based upon both the size of the crystal element used in volume averaging and the grain subdivision measure.

* Corresponding author. Tel.: +1-404-8945128; fax: +1-404-8940186.
E-mail address: david.mcdowell@me.gatech.edu (D.L. McDowell).

0020-7225/$ - see front matter © 2003 Elsevier Ltd. All rights reserved.
doi:10.1016/j.ijengsci.2003.08.001

1. Introduction

A rather large number of single crystal and polycrystal plasticity models have been proposed incorporating higher than first-order gradients (e.g., strain gradients, lattice curvature, gradient-based dislocation density measures) of deformation in the material response [1–6]. The higher order gradients render these classes of models non-local, effectively injecting a length scale (e.g., normalization constant) into the formulation on dimensional grounds, the value of which is presumably associated with a characteristic dimension of the microstructure, such as the evolving dislocation cell size in ductile FCC crystals, for example (cf. [7]).

Higher order deformation gradients have been included within plasticity theories for a variety of different reasons; we elaborate briefly on a few of these here. Their inclusion has permitted resolution of numerical difficulties associated with the solution of boundary value problems of strain softening materials in which strain localization occurs (cf. [8,9]). Gradient based approaches have also been used to model dislocation dynamics and pattern formation [10–12] and to describe single and periodic shear bands in single crystals (cf. [13]) and polycrystals [12]. Other recent applications of non-local theories include characterization of stress and strain fields, without singularities in the field variables, at dislocation cores and crack tips [14,15] and modeling the evolution of the plastic spin tensor in macroscopic finite deformation plasticity theory [16,17]. Perhaps the most recurrently reported motivation for use of gradient theories of plasticity has been representation of the observed trend of increasing strength with decreasing size of considered volume or microstructural features. Often cited is the Hall–Petch relation, in which hardness properties (i.e., yield stress and cleavage strength) increase with decreasing grain size in polycrystals (specifically an inverse square-root dependence [18,19]), a phenomenon that classical local plasticity theory, being devoid of a material length scale, is unable to capture. Shu and Fleck [20] and Forest et al. [21] used couple stress theories (pioneered by Cosserat and Cosserat [22,23]) to characterize Hall–Petch behavior in bicrystals and polycrystals, respectively. Fleck et al. [24] employed a couple stress model of strain gradient plasticity to describe an increase in flow stress with decreasing diameter of twisted thin copper wires. Shu and Fleck [25] and Hwang et al. [26] used variations of the same strain gradient-couple stress theory [27] to capture an observed increase in hardness with decreasing indentor size in pure metals.

Many theories have included a higher order gradient of elastic, plastic, or total deformation in the expression for the yield stress, slip system hardening rate, flow stress, or the backstress, with details of incorporation of gradients in the material response functions varying widely among different models. In many cases the higher order gradients are associated, upon invocation of differential-geometric arguments, with the density of "geometrically necessary dislocations" (GNDs) in single crystals (cf. [28–37]) and in polycrystals (cf. [38,16,17,9,39]). These dislocations are required to sustain the compatibility of the total deformation gradient, in contrast to the "statistically stored" dislocations (SSDs) [40] that accumulate under homogeneous plastic flow.

Physical experiments have demonstrated how the processes of grain subdivision and dislocation substructure formation substantially influence slip system activity, strain hardening, stored lattice energy, and texture evolution in single and polycrystals [41–47]. Local models have been proposed that explicitly embed subdivision and related dislocation substructure effects into the single crystal kinematics [47–50] and the hardening and grain interaction laws

of polycrystal plasticity theory [51,52], without explicitly considering the higher order gradients of deformation associated with geometrically necessary defects. Non-local solutions in terms of Green's functions [14,53] have also been developed to address defect substructure within grains and its influence on the micro-stress fields and commensurate hardening behavior. Also noteworthy is the recent approach of Ortiz and co-workers [7,54] for modeling additional internal degrees of freedom associated with dislocation substructure via a non-local sequential lamination theory. This approach permits dislocation substructure development, when energetically favorable, to occur within single crystals even under *uniform* monotonic macroscopic deformation, in contrast to many gradient-based approaches requiring heterogeneity of the deformation gradient field to drive evolution of GNDs. Such lamellar dislocation structures have been observed experimentally within ductile single crystals under monotonic loading at large deformations [42,43,55] and are thought to influence the flow stress across a wide range of temperatures and strain rates [44,56]. Carstensen et al. [57] viewed evolution of plastic flow from the standpoint of a constrained energy minimization problem and remark how heterogeneous plastic flow (e.g., subdivision or localization) may result from a lack of convexity of the free energy.

Also observed within pure ductile metals and certain alloys at large deformations and/or high temperatures are long range internal stress fields associated with misoriented subgrain boundaries [58–60]. These internal stress fields—attributed to misorientations that develop among neighboring subgrains—occur with a periodicity on the order of the subgrain size (cf. [43]). The study of Gibeling and Nix [59] found that while local internal stress fields in the unloaded configuration (i.e., residual stresses) are typically quite small compared to the average applied stress, the applied loads can alter the arrangement of subgrain walls such that the stress fields of adjacent dislocations do not cancel, thereby biasing the internal stress fields to a substantial degree.

The remainder of this work is organized as follows. Kinematics and balance laws are discussed in Sections 2 and 3, respectively, from the perspective of multiscale volume averaging. Section 4 more fully develops constitutive relations within the context of a higher order gradient, single crystal plasticity theory. In the interest of brevity, thermal effects (i.e., temperature rates and heat fluxes) and dynamic effects (i.e., acceleration and body forces) are often neglected.

We employ the following notation. Vector and tensor quantities are typically represented with boldface type, while scalars and individual components of vectors and tensors are written in italics. The index notation is often used for clarity, following the Einstein summation convention and distinguishing between covariant (subscript) and contravariant (superscript) components. Current configuration indices are written in lower case Latin, reference configuration indices in upper case Latin, and intermediate configuration indices are written using Greek symbols. Juxtaposition implies summation over two repeated adjacent indices (e.g., $(\mathbf{AB})^{\cdot b}_{a} = A_{ac}B^{cb}$). The dot (scalar) product of vectors is represented by the symbol "$\cdot$" (e.g., $\mathbf{a}\cdot\mathbf{b} = a^{a}g_{ab}b^{b}$, with g_{ab} components of the metric tensor). Angled brackets denote a dual (scalar) product (e.g., for second-rank tensors, $\langle \mathbf{A}, \mathbf{B}\rangle = \mathrm{tr}(\mathbf{AB}) = A_{ab}B^{ba}$, and for contra covector pairs, $\langle \boldsymbol{\alpha}, \mathbf{b}\rangle = \alpha_{a}b^{a}$). The colon denotes contraction over repeated pairs of indices (e.g., $\mathbf{A}:\mathbf{B} = \mathrm{tr}(\mathbf{A}^{T}\mathbf{B}) = A_{ab}B^{ab}$ and $\mathbf{C}:\mathbf{E} = C^{abcd}E_{cd}$). The symbol "$\otimes$" represents the tensor (outer) product (e.g., $(\mathbf{a}\otimes\mathbf{b})^{ab} = a^{a}b^{b}$). Superposed -1, T, and "$\cdot$" denote inverse, transpose, and material time derivative operations, respectively. Additional notation is clarified as needed later in the text.

2. Multiscale kinematics

A fundamental difference between the model developed in the present work and the numerous strain gradient approaches already cited is our usage of rigorous volume averaging procedures to characterize the kinematics of elasto(visco)plastic deformation. Continuum elements (i.e., domains for volume integration) representing a deforming crystal or region within are shown in Fig. 1. The symbols v_{ref}, $\tilde{v}_{\text{int}}$, and v_{cur} denote volume elements in reference, intermediate, and current configurations. Dimensions of v_{ref} are assumed to adhere to

$$a_0 \ll \ell_{\text{ref}} \leqslant L_{\text{G}}, \tag{1}$$

with a_0 and L_{G} the lattice parameter and average grain diameter, respectively, and with $\ell_{\text{ref}} \equiv \sqrt[3]{v_{\text{ref}}}$. We also frequently invoke the following notation for configurations at multiple length scales: $v_{\text{ref}} \equiv b_{\text{ref}} \subset B_{\text{ref}}$, $\tilde{v}_{\text{int}} \equiv \tilde{b}_{\text{int}} \subset \widetilde{B}_{\text{int}}$, and $v_{\text{cur}} \equiv b_{\text{cur}} \subset B_{\text{cur}}$, where *global* reference, intermediate, and current configurations of the entire macroscopic body are labeled B_{ref}, $\widetilde{B}_{\text{int}}$, and B_{cur}. All configurations will be described in more detail later in the text. Local, scalar "differential" volume elements within reference, intermediate, and current configurations are labeled $\mathrm{d}v_{\text{ref}}$, $\mathrm{d}\tilde{v}_{\text{int}}$, and $\mathrm{d}v_{\text{cur}}$, respectively. Differential elements are required to be smaller than their associated volume elements, but not necessarily infinitesimal in size.

The motion of points of the body from the reference to current configuration is written

$$x^a = \boldsymbol{\varphi}^a(X^A, t) \quad (a, A = 1, 2, 3), \tag{2}$$

where x^a, X^A, and t denote, respectively, current configuration coordinates, reference configuration coordinates, and time. The local motion $\boldsymbol{\varphi}^a$ is assumed to be continuously differentiable within v_{cur}. *Local* intermediate configuration coordinates are also assumed to be continuous *within* $\tilde{v}$. These are denoted by $\tilde{x}^\alpha = \tilde{x}^\alpha(X^A, t)(\alpha = 1, 2, 3)$. Further remarks on the availability of continuous, single-valued coordinates $\tilde{x}^\alpha$ follow later.

Basis vectors in each configuration are labeled as

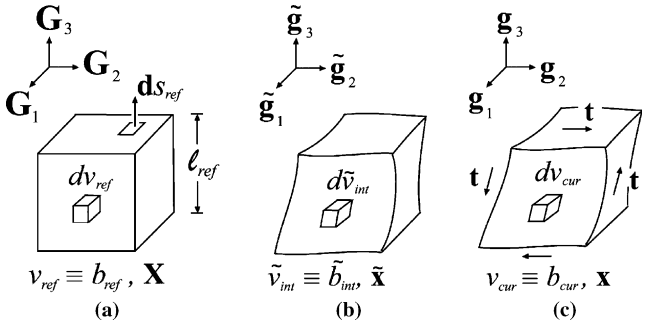

Fig. 1. Configurations, differential volumes, and coordinate systems for crystal volume element: (a) reference, (b) intermediate, and (c) current.

$$\mathbf{G}_A \equiv \frac{\partial}{\partial X^A}, \quad \tilde{\mathbf{g}}_\alpha \equiv \frac{\partial}{\partial \tilde{x}^\alpha}, \quad \mathbf{g}_a \equiv \frac{\partial}{\partial x^a}. \tag{3}$$

Basis covectors (i.e., dual vectors) are introduced as

$$\mathbf{G}^A \equiv \mathbf{d}X^A, \quad \tilde{\mathbf{g}}^\alpha \equiv \mathbf{d}\tilde{x}^\alpha, \quad \mathbf{g}^a \equiv \mathbf{d}x^a, \tag{4}$$

satisfying

$$\langle \mathbf{G}^A, \mathbf{G}_B \rangle = \delta^A_B, \quad \langle \tilde{\mathbf{g}}^\alpha, \tilde{\mathbf{g}}_\beta \rangle = \delta^\alpha_\beta, \quad \langle \mathbf{g}^a, \mathbf{g}_b \rangle = \delta^a_b. \tag{5}$$

Metric tensors are introduced on each configuration, obeying the relations

$$G_{AB} = \mathbf{G}_A \cdot \mathbf{G}_B, \quad \tilde{g}_{\alpha\beta} = \tilde{\mathbf{g}}_\alpha \cdot \tilde{\mathbf{g}}_\beta, \quad g_{ab} = \mathbf{g}_a \cdot \mathbf{g}_b. \tag{6}$$

The notation $G \equiv \det \mathbf{G}$, $\tilde{g} \equiv \det \tilde{\mathbf{g}}$, and $g \equiv \det \mathbf{g}$ denotes determinants of metric tensors given in (6). Since we often use volume averaging operations over the crystal element to define certain tensorial quantities, we restrict the basis vectors (3), basis covectors (4), and metric tensors (6) to be constant, but not necessarily Cartesian, within each element (i.e., v_{ref}, $\tilde{v}_{\text{int}}$, and v_{cur}) in each configuration, such that covariant and partial differentiation are equivalent operations. However, these variables are permitted to vary from volume element to volume element (if curvilinear coordinates are useful), and also from configuration to configuration.

The configurations of the crystalline volume element shown in Fig. 1 are now defined in turn. The reference configuration volume v_{ref} consists of the crystalline lattice as it existed prior to application of external forces (i.e., at $t = 0$), such that it is free of traction along the external boundary s_{ref}. It may or may not contain dislocations, internal residual elastic lattice strains, or residual plastic deformation. The current configuration volume element, v_{cur}, is the elastoplastically-deformed crystal material, with possibly non-vanishing traction vector $\mathbf{t}$ per unit reference area applied on external boundary s_{cur}.

The local deformation gradient $\mathbf{f}$ for material points with local coordinates X^A within the volume element is defined as the tangent mapping

$$\mathbf{f} \equiv T\boldsymbol{\varphi}_X = \frac{\partial \boldsymbol{\varphi}^a}{\partial X^A} \mathbf{g}_a \otimes \mathbf{G}^A. \tag{7}$$

The volume-averaged deformation gradient $\mathbf{F}$ for the crystal element is then defined by the motion of its external boundary, which is equivalent to the volume-averaged local deformation gradient upon invocation of Gauss's theorem [61]:

$$F^a_{\cdot A} \equiv \frac{1}{v_{\text{ref}}} \int_{s_{\text{ref}}} x^a (\mathrm{d}s_{\text{ref}})_A = \frac{1}{v_{\text{ref}}} \int_{s_{\text{ref}}} \frac{\partial x^a}{\partial X^A} \, \mathrm{d}v_{\text{ref}} = \frac{1}{v_{\text{ref}}} \int_{s_{\text{ref}}} f^a_{\cdot A} \, \mathrm{d}v_{\text{ref}}. \tag{8}$$

In Eq. (8), $(\mathrm{d}s_{\text{ref}})_A \equiv (n_{\text{ref}})_A \mathrm{d}s_{\text{ref}}$ is an oriented differential surface element of s_{ref} (Fig. 1), with $\mathbf{n}_{\text{ref}}$ a unit covariant vector normal to s_{ref}.

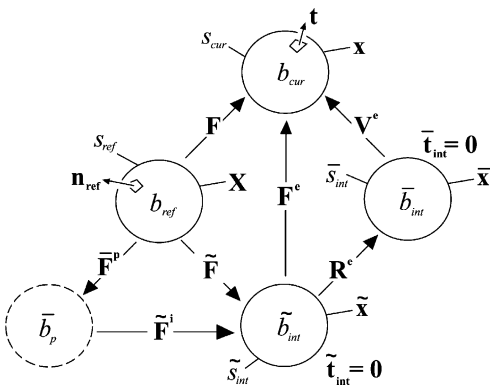

Fig. 2. Configurations for crystal volume element.

An average elastic stretch tensor $\mathbf{V}^e$ is associated with the average external stress applied to s_{cur}. The intermediate configuration $\bar{b}_{int}$ (Fig. 2) of the crystal element reached upon hypothetical instantaneous elastic unloading from the current configuration via the inverse of the elastic stretch $\mathbf{V}^{e-1}$ corresponds to null traction conditions on the external boundary of the crystal volume element $\bar{v}_{int}$ (i.e., the traction $\bar{\mathbf{t}}_{int} = \mathbf{0}$ along $\bar{s}_{int}$), as shown in Fig. 2. The left elastic stretch tensor $\mathbf{V}^e$ is determined explicitly from

$$\mathbf{V}^e = \left(\int_{s_{ref}} \mathbf{x} \otimes \mathbf{d}s_{ref} \right) \left(\int_{s_{ref}} \bar{\mathbf{x}} \otimes \mathbf{d}s_{ref} \right)^{-1}, \tag{9}$$

where $\bar{\mathbf{x}}$ are the local coordinates of the external boundary of the element corresponding to traction-free intermediate configuration $\bar{b}_{int}$. Configuration $\bar{b}_{int}$ arises from instantaneous removal of traction along the boundary of $\bar{v}_{int}$, constrained in such a way that the global rotation of the volume element, $\mathbf{R}^{e-1}$, does not occur upon stress relaxation. Upon unloading, plastic rearrangements are idealized as rate independent and inertial effects are neglected.

The total "elastic" rotation tensor $\mathbf{R}^e$ is determined from the solution of the following integro-differential equation for the elastic spin and associated initial conditions:

$$\dot{\mathbf{R}}^e \mathbf{R}^{e-1} = \frac{1}{v_{ref}} \int_{v_{ref}} \dot{\mathbf{r}}^e \mathbf{r}^{e-1} \, \mathrm{d}v_{ref}, \quad \mathbf{R}^e(t=0) = \mathbf{r}^e(t=0) = \mathbf{1}, \tag{10}$$

where $\mathbf{1}$ is the identity map and $\mathbf{r}^e$ is the local elastic and rigid body rotation exhibited by $\mathrm{d}v_{ref}$ as it is deformed to its current representation $\mathrm{d}v_{cur}$. Note that $\mathbf{R}^{eT} = \mathbf{R}^{e-1}$ follows from (10) and $\mathbf{r}^{eT} = \mathbf{r}^{e-1}$, since volume averaging preserves the anti-symmetric property of the spin.

The intermediate configuration $\tilde{b}_{int}$ is defined by the net unloading procedure $\mathbf{F}^{e-1} = \mathbf{R}^{eT}\mathbf{V}^{e-1}$, i.e. unloading by the external forces and subsequent rotation by the inverse (i.e., transpose) of the average lattice rotation. After this unloading procedure, local coordinates $\tilde{x}^\alpha$ describe the positions of particles *within* the volume element $\tilde{v}_{int}$. The local residual deformation gradient $\tilde{\mathbf{f}}$ is the tangent mapping

$$\tilde{\mathbf{f}} \equiv T\tilde{\boldsymbol{\varphi}}_X = \frac{\partial \tilde{\boldsymbol{\varphi}}^{\alpha}}{\partial X^A}\tilde{\mathbf{g}}_{\alpha} \otimes \mathbf{G}^A, \tag{11}$$

with $\tilde{x}^{\alpha} = \tilde{\boldsymbol{\varphi}}^{\alpha}(x^a(X^A,t),t)$ the motion for differential volume elements between b_{ref} and $\tilde{b}_{\text{int}}$. The volume-averaged residual deformation gradient $\widetilde{\mathbf{F}}$ for the crystal element is deduced from the intermediate configuration coordinates of its external boundary, and is equivalent to the volume-averaged residual local deformation gradient upon invocation of Gauss's theorem (compare with (8))

$$\widetilde{F}^{\alpha}_{\cdot A} \equiv \frac{1}{v_{\text{ref}}}\int_{s_{\text{ref}}} \tilde{x}^{\alpha}(\mathrm{d}s_{\text{ref}})_A = \frac{1}{v_{\text{ref}}}\int_{s_{\text{ref}}} \frac{\partial \tilde{x}^{\alpha}}{\partial X^A}\,\mathrm{d}v_{\text{ref}} = \frac{1}{v_{\text{ref}}}\int_{s_{\text{ref}}} \tilde{f}^{\alpha}_{\cdot A}\,\mathrm{d}v_{\text{ref}}. \tag{12}$$

We now make two additional assumptions regarding the kinematics of single crystalline elastoplasticity on a "pointwise" basis, for each differential volume element [62]

$$\mathbf{f} = \mathbf{f}^{\mathrm{e}}\mathbf{f}^{\mathrm{p}}, \quad \tilde{\mathbf{f}} = \tilde{\mathbf{f}}^{\mathrm{e}}\tilde{\mathbf{f}}^{\mathrm{p}}. \tag{13}$$

In Eq. $(13)_1$, $\mathbf{f}^{\mathrm{e}} = \mathbf{v}^{\mathrm{e}}\mathbf{r}^{\mathrm{e}}$ is the total lattice stretch ($\mathbf{v}^{\mathrm{e}}$) and rotation ($\mathbf{r}^{\mathrm{e}}$) for a differential volume element deformed to the current configuration, and $\mathbf{f}^{\mathrm{p}}$ is the remaining (plastic) deformation gradient attributed to the history of motion of dislocations. In Eq. $(13)_2$, $\tilde{\mathbf{f}}^{\mathrm{e}}$ embodies the residual elastic lattice stretch and rotation for a differential volume element contained within the externally unloaded element $\tilde{v}_{\text{int}}$, and $\tilde{\mathbf{f}}^{\mathrm{p}}$ is the residual plastic deformation gradient arising from dislocation motion. In order to illustrate (13), we label differential volume elements as $\mathrm{d}v_{\text{ref}} \subset v_{\text{ref}}$, $\mathrm{d}\tilde{v}_{\text{int}} \subset \tilde{v}_{\text{int}}$, and $\mathrm{d}v_{\text{cur}} \subset v_{\text{cur}}$ in Fig. 3 with differential elements visually enlarged relative to their surrounding crystal volume elements for clarity. The local deformation gradients of (13) then act as mappings between tangent spaces of local "differential configurations":

$$\begin{aligned} &\mathbf{f} : T(\mathrm{d}v_{\text{ref}}) \to T(\mathrm{d}v_{\text{cur}}), \quad \mathbf{f}^{\mathrm{p}} : T(\mathrm{d}v_{\text{ref}}) \to T(\mathrm{d}v_{\mathrm{p}}), \quad \mathbf{f}^{\mathrm{e}} : T(\mathrm{d}v_{\mathrm{p}}) \to T(\mathrm{d}v_{\text{cur}}),\\ &\tilde{\mathbf{f}} : T(\mathrm{d}v_{\text{ref}}) \to T(\mathrm{d}\tilde{v}_{\text{int}}), \quad \tilde{\mathbf{f}}^{\mathrm{p}} : T(\mathrm{d}v_{\text{ref}}) \to T(\mathrm{d}\tilde{v}_{\mathrm{p}}), \quad \tilde{\mathbf{f}}^{\mathrm{e}} : T(\mathrm{d}\tilde{v}_{\mathrm{p}}) \to T(\mathrm{d}\tilde{v}_{\text{int}}), \end{aligned} \tag{14}$$

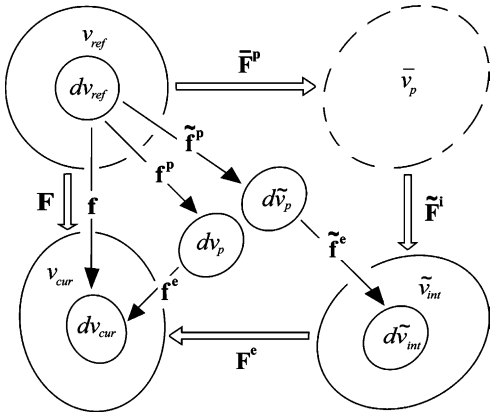

Fig. 3. Tangent mappings and volume elements at multiple length scales.

Notice that of the six tangent mappings in (14), only $\mathbf{f}$ and $\tilde{\mathbf{f}}$ are necessarily compatible deformation gradient fields, in agreement with definitions (7) and (11).

The total plastic deformation gradient $\overline{\mathbf{F}}^{\mathrm{p}}$ for the volume element emerges from the following integro-differential equation written in terms of the plastic velocity gradient:

$$\dot{\overline{\mathbf{F}}}^{\mathrm{p}}\overline{\mathbf{F}}^{\mathrm{p}-1} \equiv \frac{1}{v_{\mathrm{ref}}}\int_{v_{\mathrm{ref}}} \dot{\mathbf{f}}^{\mathrm{p}}\mathbf{f}^{\mathrm{p}-1}\,\mathrm{d}v_{\mathrm{ref}}, \tag{15}$$

with initial conditions $\overline{\mathbf{F}}^{\mathrm{p}}(t=0) = \mathbf{f}^{\mathrm{p}}(t=0) = \mathbf{1}$ if a perfect reference lattice is assumed. Notice that if the local plastic flow is isochoric, i.e. $\mathrm{tr}(\dot{\mathbf{f}}^{\mathrm{p}}\mathbf{f}^{\mathrm{p}-1}) = 0$, then the volume-averaged plastic flow of (15) is volume-preserving as well, i.e. $\mathrm{tr}(\dot{\overline{\mathbf{F}}}^{\mathrm{p}}\overline{\mathbf{F}}^{\mathrm{p}-1}) = 0$.

Next we assume a three-term multiplicative decomposition for the total deformation $\mathbf{F}$:

$$\mathbf{F} = \mathbf{F}^{\mathrm{e}}\underbrace{\widetilde{\mathbf{F}}^{\mathrm{i}}\overline{\mathbf{F}}^{\mathrm{p}}}_{\widetilde{\mathbf{F}}} = \mathbf{F}^{\mathrm{e}}\widetilde{\mathbf{F}}, \tag{16}$$

where the net residual deformation gradient $\widetilde{\mathbf{F}}$ enters the decomposition as shown, in accordance with our previous definitions of $\mathbf{F}^{\mathrm{e}}$ and $\widetilde{\mathbf{F}}$. Combining Eqs. (8), (12), $(13)_2$, and (16) leads to the definition of $\widetilde{\mathbf{F}}^{\mathrm{i}}$:

$$\widetilde{\mathbf{F}}^{\mathrm{i}} \equiv \widetilde{\mathbf{F}}\overline{\mathbf{F}}^{\mathrm{p}-1} = \frac{1}{v_{\mathrm{ref}}}\left(\int_{v_{\mathrm{ref}}} \tilde{\mathbf{f}}^{\mathrm{e}}\tilde{\mathbf{f}}^{\mathrm{p}}\mathrm{d}v_{\mathrm{ref}}\right)\overline{\mathbf{F}}^{\mathrm{p}-1}. \tag{17}$$

The $\widetilde{\mathbf{F}}^{\mathrm{i}}$ (two-point) tensor can be thought of as an indicator of residual elasticity in configuration $\tilde{b}_{\mathrm{int}}$ (and corresponding residual stresses and interaction energies). The deformation tensor $\widetilde{\mathbf{F}}^{\mathrm{i}}$ contains both residual elastic ($\tilde{\mathbf{f}}^{\mathrm{e}}$) and plastic ($\tilde{\mathbf{f}}^{\mathrm{p}}, \overline{\mathbf{F}}^{\mathrm{p}}$) contributions. It is clear from Eq. $(17)_2$ that $\widetilde{\mathbf{F}}^{\mathrm{i}} \to \mathbf{1}$ as $\tilde{\mathbf{f}}^{\mathrm{e}} \to \mathbf{1}$ and $\tilde{\mathbf{f}}^{\mathrm{p}} \to \overline{\mathbf{F}}^{\mathrm{p}}$, as would be the case for homogeneous deformation of the entire crystalline element, such that external unloading by $\mathbf{V}^{\mathrm{e}-1}$ relieves all local internal stresses and plastic rearrangements do not occur upon instantaneous unloading. On the other hand, if the elastoplastic deformation fields are heterogeneous throughout the volume element, $\widetilde{\mathbf{F}}^{\mathrm{i}}$ and commensurate residual stresses may not vanish. Such is the case when cellular or laminar dislocation substructures misoriented from one other by finite lattice rotations (embodied here locally by the orthogonal part $\tilde{\mathbf{r}}^{\mathrm{e}}$ of $\tilde{\mathbf{f}}^{\mathrm{e}}$) evolve and refine during large strain deformations in FCC metals at room temperatures [43,44]. When the volume element encompasses an entire single crystal ($\ell_{\mathrm{ref}} = L_{\mathrm{G}}$ in Eq. (1)), we thus conclude that $\widetilde{\mathbf{F}}^{\mathrm{i}}$ represents *the contribution of grain subdivision* processes to the total deformation gradient $\mathbf{F}$ for the crystal, as originally proposed by Butler and McDowell [50]. Additionally, if heterogeneity of local deformation and stresses due to elastoplastic incompatibility (e.g., increased slip system activity and stress concentrations) are intensified in the vicinity of misoriented grain and subgrain boundaries (cf. experimental and numerical results in [62]), then one would expect the largest contributions to $\widetilde{\mathbf{F}}^{\mathrm{i}}$ to come from these regions.

The deformation tensor $\widetilde{\mathbf{F}}^{\mathrm{i}}$ represents in an average sense the incompatibility of the local microelastic deformation $\mathbf{f}^{\mathrm{e}-1}$ *within the volume element*. If the local elastic unloading $\mathbf{f}^{\mathrm{e}-1}$ is uniform (and hence, compatible) throughout v_{cur}, then $\mathbf{f}^{\mathrm{e}} = \mathbf{F}^{\mathrm{e}}$, $\tilde{\mathbf{f}}^{\mathrm{e}} = \mathbf{1}$, and $\widetilde{\mathbf{F}} = \tilde{\mathbf{f}} = \overline{\mathbf{F}}^{\mathrm{p}} = \tilde{\mathbf{f}}^{\mathrm{p}} = \mathbf{f}^{\mathrm{p}}$, such that $\widetilde{\mathbf{F}}^{\mathrm{i}} = \mathbf{1}$ (Fig. 3). However, $\widetilde{\mathbf{F}}^{\mathrm{i}}$ tells us nothing about the compatibility, or lack thereof, of the

average recoverable elastic deformation $\mathbf{F}^{\mathrm{e}-1}$ from volume element to volume element. If we regard each v_{ref} as an entire single crystal, then the incompatibility of $\mathbf{F}^{\mathrm{e}-1}$ measures the intergranular incompatibility between grains, while if we regard each v_{ref} as a subgrain, then the incompatibility of $\mathbf{F}^{\mathrm{e}-1}$ is an intragranular measure. By incompatibility of $\mathbf{F}^{\mathrm{e}-1}$ we mean lack of continuous, single-valued coordinates $\tilde{x}^{\alpha}$ spanning the union of i local intermediate configuration volume elements $\widetilde{V}_{\mathrm{int}} \equiv \cup \tilde{v}^{(i)}_{\mathrm{int}}$. Thus, while the $\tilde{x}^{\alpha}$ are assumed to be available and differentiable within each local volume element $\tilde{v}^{(i)}_{\mathrm{int}}$, they may not be so in the global configuration $\widetilde{B}_{\mathrm{int}} \equiv \widetilde{V}_{\mathrm{int}}$. If the $\tilde{x}^{\alpha}$ are multi-valued or discontinuous in the global configuration, they are typically called anholonomic coordinates [63].

We now appeal to the continuum theories of continuously distributed dislocations [64–66] to characterize the incompatibility of *global* configuration $\widetilde{B}_{\mathrm{int}}$ (i.e., the anholonomicity or lack of integrability of $\mathbf{F}^{\mathrm{e}-1}$). The coefficients $\overline{\Gamma}^{a}_{bc}$ of the "crystal connection" (cf. [31,67]) acquire the following form when referred to the current configuration:

$$\overline{\Gamma}^{a}_{bc} = F^{e^a}_{\cdot\alpha}\frac{\partial F^{e-1^{\alpha}}}{\partial x^b} = F^{\mathrm{e}^a}_{\cdot\alpha}F^{\mathrm{e}-1^{\alpha}}_{\cdot c,b} = -F^{e-1^{\alpha}}_{\cdot c}F^{e^a}_{\cdot\alpha,b}, \tag{18}$$

with the subscripted comma denoting partial differentiation with respect to spatial coordinates as indicated. In (18) we require $\mathbf{F}^{\mathrm{e}-1}$ to be spatially differentiable to first-order; thus, for the present discussion, local misorientations across grain and subgrain boundaries (i.e., between volume elements v_{cur}) are envisioned as steep gradients of lattice rotation, as opposed to actual discontinuities in the lattice arrangement. The torsion of the connection $\overline{\Gamma}^{a}_{bc}$ is written

$$\bar{\mathbf{t}} = -2F^{\mathrm{e}^a}_{\cdot\alpha}F^{\mathrm{e}-1^{\alpha}}_{\cdot[b,c]}\mathbf{g}_a \otimes \mathbf{g}^b \otimes \mathbf{g}^c = -2F^{\mathrm{e}^a}_{\cdot\alpha}F^{\mathrm{e}-1^{\alpha}}_{\cdot[b\,|\,c]}\mathbf{g}_a \otimes \mathbf{g}^b \otimes \mathbf{g}^c, \tag{19}$$

where we have replaced partial differentiation (subscripted comma) with partial covariant differentiation with respect to the Levi-Civita connection on B_{cur} whose Christoffel symbols stem from the components of the metric g_{ab} of Eq. $(6)_3$ and thus are symmetric in covariant indices. We use the notation of vertical bars for such covariant differentiation. Additionally, the bracketed indices are anti-symmetrized according to $2A_{[ab]} = A_{ab} - A_{ba}$.

We now relate the torsion tensor $\bar{\mathbf{t}}$ of Eq. (19) to the anholonomicity of the inverse elastic deformation gradient field $\mathbf{F}^{\mathrm{e}-1}$. The incompatibility of regions within global configuration $\widetilde{B}_{\mathrm{int}}$ is associated with the net Burgers vector $\widetilde{\mathbf{B}}$, defined in terms of the closure failure of the line integral of $\mathrm{d}\tilde{\mathbf{x}} \equiv \mathbf{F}^{\mathrm{e}-1}\,\mathrm{d}\mathbf{x}$ over a closed loop $\tilde{c}$ in $\widetilde{B}_{\mathrm{int}}$ [65,66]

$$\widetilde{\mathbf{B}} \equiv -\oint_{\tilde{c}} \mathrm{d}\tilde{\mathbf{x}} = -\oint_{c} \mathbf{F}^{\mathrm{e}-1}\,\mathrm{d}\mathbf{x}. \tag{20}$$

Applying Stokes' theorem (cf. [4]), we express Eq. (20) as

$$-\oint_{c} F^{\mathrm{e}-1^{\alpha}}_{\cdot a}\mathrm{d}x^a = \int_a F^{\mathrm{e}-1^{\alpha}}_{\cdot[a\,|\,b]}\,\mathrm{d}x^a \wedge \mathrm{d}x^b = \int_a \varepsilon^{abc}F^{\mathrm{e}-1^{\alpha}}_{\cdot a,b}n_c\,\mathrm{d}a, \tag{21}$$

where $\mathrm{d}x^a \wedge \mathrm{d}x^b = \varepsilon^{abc}n_c\,\mathrm{d}a = \sqrt{g}e^{abc}n_c\,\mathrm{d}a$ is the differential area two-form corresponding to oriented area element $\mathbf{n}\,\mathrm{d}a$ bounded by curve c (Fig. 4), which in turn is the current configuration

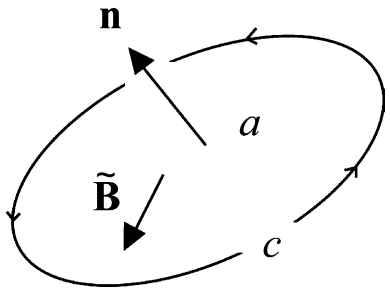

Fig. 4. Burgers circuit in current configuration.

image of Burgers circuit $\tilde{c}$. The wedge product is denoted by $\wedge$, and components of the contravariant permutation tensor (i.e., alternator tensor) in the current configuration are denoted by $\varepsilon^{abc} = (\sqrt[-1]{g})e^{abc}$, with e^{abc} the standard permutation symbols.

The incompatibility is expressed in terms of the torsion of the crystal connection by combining (18)–(21)$_1$, i.e.

$$\widetilde{B}^{\alpha} = -\frac{1}{2}\int_a F^{\mathrm{e}-1\,\alpha}_{\cdot c}\,\overset{\mathrm{c}}{t}_{ab}\,\mathrm{d}x^a \wedge \mathrm{d}x^b. \tag{22}$$

By defining the operator

$$\mathrm{curl}(\cdot) \equiv (\partial(\cdot)/\partial\mathbf{x}) : \boldsymbol{\varepsilon}, \tag{23}$$

we may write for (21)$_2$

$$\widetilde{\mathbf{B}} = \int_a \mathrm{curl}(\mathbf{F}^{\mathrm{e}-1}) \cdot \mathbf{n}\,\mathrm{d}a = \int_a \mathbf{A}^{\mathrm{e}} \cdot \mathbf{n}\,\mathrm{d}a, \tag{24}$$

where $\mathbf{A}^{\mathrm{e}} \equiv \mathrm{curl}(\mathbf{F}^{\mathrm{e}-1})$ and the vector $\mathbf{n}\,\mathrm{d}a = (n^a\,\mathrm{d}a)\mathbf{g}_a$. Invoking Nanson's formula $\tilde{\mathbf{n}}\mathrm{d}\tilde{a} = J^{\mathrm{e}-1}\mathbf{n}\cdot\mathbf{F}^{\mathrm{e}}\,\mathrm{d}a$ (cf. [35]), we can transform (24) to an area integral over an intermediate configuration region $\tilde{a}$

$$\widetilde{\mathbf{B}} = \int_{\tilde{a}} \tilde{\mathbf{n}} \cdot \underbrace{J^{\mathrm{e}}\mathbf{F}^{\mathrm{e}-1}\mathbf{A}^{\mathrm{e}\mathrm{T}}}_{\widetilde{\mathbf{A}^{\mathrm{e}}}}\,\mathrm{d}\tilde{a} = \int_{\tilde{a}} \tilde{\mathbf{n}} \cdot \tilde{\mathbf{A}}^{\mathrm{e}}\mathrm{d}\tilde{a}, \tag{25}$$

where the dot product in the integrand of (25) denotes contraction of the covariant index of $\tilde{\mathbf{n}}$ with the contravariant index of $\mathbf{F}^{\mathrm{e}-1}$. Note that $\tilde{\mathbf{A}}^{\mathrm{e}}$ only measures GNDs and does not account for SSDs (e.g., closed dislocation loops) within v_{ref} [68,69].

Discussion regarding the length scales inherent in the line integral (20) is now in order. Two distinct length scales are included in the integral (20) and are intimately related. One is the choice of size of $\tilde{c}$: we let $D(\tilde{c})$ denote the diameter of a circle equivalent to $\tilde{c}$. The other is the choice of ℓ_{ref}, which defines the size of the volume element $v_{\mathrm{ref}} = \ell^3_{\mathrm{ref}}$, and thus $\tilde{v}_{\mathrm{int}}$, and implicitly affects the definition of the average elastic deformation gradient for the element, $\mathbf{F}^{\mathrm{e}}$. Eq. (20) is really valid

only for $D(\tilde{c}) \geqslant l_{\text{ref}}$, if we take ℓ_{ref} to be a characteristic diameter of the volume element $\tilde{v}_{\text{int}}$ considered. Under this condition, $\mathbf{F}^{\text{e}}$ and its gradient are defined in regions within circuit $\tilde{c}$. If the converse is true, such that $D(\tilde{c}) < \ell_{\text{ref}}$, we need to consider the incompatibility of the inverse *microelastic* deformation within the volume element, $\mathbf{f}^{\text{e}-1}$, instead since $\mathbf{F}^{\text{e}-1}$ is not defined *within* the volume element. Repeating the derivation leading up to (24) for the microelastic deformation $\mathbf{f}^{\text{e}-1}$, we arrive at an expression for a local Burgers vector $\tilde{\mathbf{b}}^{\text{e}}$

$$\tilde{\mathbf{b}}^{\text{e}} \equiv -\oint_c \mathbf{f}^{\text{e}-1}\mathrm{d}\mathbf{x} = \int_a \operatorname{curl}(\mathbf{f}^{\text{e}-1}) \cdot \mathbf{n}\,\mathrm{d}a. \tag{26}$$

Notice that $\tilde{\mathbf{b}}^{\text{e}} = \tilde{b}^{\text{e}\bar{\alpha}}\tilde{\mathbf{g}}_{\bar{\alpha}} \in T(\mathrm{d}v_{\text{p}})$ resides in a different tangent space than the vector $\widetilde{\mathbf{B}}$ of (25). We use barred Greek indices to denote components in this space, which arises from the local plastic deformation $\mathbf{f}^{\text{p}}$, as shown in Fig. 3. Under certain conditions we can further characterize (26) in terms of the spatial gradient of the inverse of the residual elastic deformation gradient $\tilde{\mathbf{f}}^{\text{e}}$. Since both $\mathrm{d}\tilde{v}_{\text{int}}$ and $\mathrm{d}v_{\text{cur}}$ inhabit local volume elements deformed in a compatible fashion, we can define a local compatible tangent mapping between them: $\bar{\mathbf{f}}^{\text{c}-1} \equiv \frac{\partial \tilde{\mathbf{x}}}{\partial \mathbf{x}} : T(\mathrm{d}v_{\text{cur}}) \to T(\mathrm{d}\tilde{v}_{\text{int}})$. If no additional local plastic deformation occurs upon external unloading of the volume element, in the process symbolized by $\mathbf{F}^{\text{e}-1}$, then microscopically we have $\mathbf{f}^{\text{p}} = \tilde{\mathbf{f}}^{\text{p}}$ and $\mathrm{d}v_{\text{p}} = \mathrm{d}\tilde{v}_{\text{p}}$, as shown in Fig. 5. Furthermore, we may write

$$\mathbf{f}^{\text{e}} = \bar{\mathbf{f}}^{\text{c}}\tilde{\mathbf{f}}^{\text{e}}, \tag{27}$$

thereby decomposing the total microelastic deformation into a residual part $\tilde{\mathbf{f}}^{\text{e}}$ and a compatible part $\bar{\mathbf{f}}^{\text{c}}$ due to the applied stress [70]. Substituting (27) into (26) and invoking the compatibility conditions $\bar{f}^{\text{c}-1\beta}_{\cdot[a,b]} = 0$ then gives

$$\tilde{b}^{\text{e}\bar{\alpha}} = \int_a \varepsilon^{cab}(\tilde{f}^{\text{e}-1\bar{\alpha}}_{\cdot\beta,b}\bar{f}^{\text{c}-1\beta}_{\cdot a} + \tilde{f}^{\text{e}-1\bar{\alpha}}_{\cdot\beta}\bar{f}^{\text{c}-1\beta}_{\cdot a,b})n_c\,\mathrm{d}a = \int_a \varepsilon^{cab}(\tilde{f}^{e-1\bar{\alpha}}_{\cdot\beta,b}\bar{f}^{\text{c}-1\beta}_{\cdot a})n_c\,\mathrm{d}a, \tag{28}$$

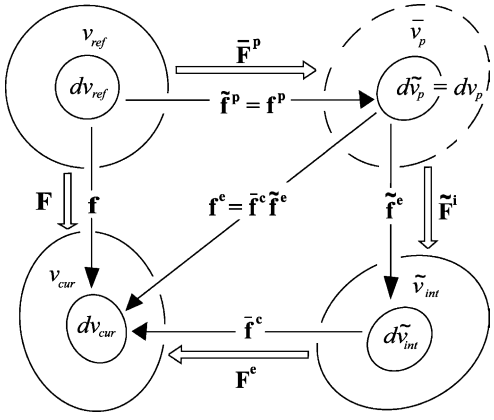

Fig. 5. Tangent mappings and volume elements when $\mathbf{f}^{\text{p}} = \tilde{\mathbf{f}}^{\text{p}}$.

demonstrating that $\tilde{\mathbf{b}}^{\mathrm{e}}$ of Eq. (26), representing the anholonomicity of the local elastic deformation gradient, depends only upon the spatial gradient of the (inverse of the) residual elastic lattice deformation map $\tilde{\mathbf{f}}^{\mathrm{e}}$. and not higher order gradients of the locally compatible and recoverable elastic lattice deformation field $\bar{\mathbf{f}}^{\mathrm{e}}$.

3. Multiscale balance laws

Neglecting body forces, let the crystal element be subjected to arbitrary but self-equilibrating surface traction $\mathbf{t}$, measured per unit area in the reference configuration, with corresponding outward unit normal covector $\mathbf{n}_{\mathrm{ref}}$ (Fig. 2). Let s^{Aa} represent the contravariant components of the local two-point nominal stress tensor (the transpose of the first Piola–Kirchhoff stress tensor). The traditional (non-polar) local balances of linear and angular momentum, respectively, are written for quasi-static conditions as

$$s^{Aa}_{|A} = 0, \quad f^{a}_{\cdot A} S^{Ab} = S^{Aa} f^{b}_{\cdot A}, \tag{29}$$

with $n_{\mathrm{ref}} A^{S^{Aa}} = t^{a}$ on S_{ref}, and with the vertical bar denoting covariant differentiation with respect to the symmetric Levi–Civita connection on b_{ref}. Notice that Eq. (29) are applicable locally, for points (i.e., differential elements) within the crystal element. We next define the average nominal stress tensor for the volume element as (cf. [71])

$$\mathbf{S} \equiv \frac{1}{v_{\mathrm{ref}}} \int_{v_{\mathrm{ref}}} \mathbf{s}\, \mathrm{d}v_{\mathrm{ref}} = \frac{1}{v_{\mathrm{ref}}} \int_{s_{\mathrm{ref}}} \mathbf{X} \otimes \mathbf{t}\, \mathrm{d}s_{\mathrm{ref}}, \tag{30}$$

where Gauss's theorem has been used for Eq. $(30)_2$, along with the assumptions of quasi-static conditions, Eq. $(29)_1$, and stress continuity within the volume element. The definition of the contravariant Cauchy stress $\boldsymbol{\Sigma}$ then follows as

$$\Sigma^{ab} \equiv J^{-1} F^{a}_{\cdot A} S^{Ab}, \tag{31}$$

with $J \equiv \det\mathbf{F}\sqrt{g/G}$. The macroscopic rate of the deformation gradient, $\dot{\mathbf{F}}$, is given by

$$\dot{\mathbf{F}} \equiv \frac{1}{v_{\mathrm{ref}}} \int_{v_{\mathrm{ref}}} \dot{\mathbf{f}}\, \mathrm{d}v_{\mathrm{ref}} = \frac{\mathrm{d}}{\mathrm{d}t}\left(\frac{1}{v_{\mathrm{ref}}} \int_{v_{\mathrm{ref}}} \mathbf{f}\, \mathrm{d}v_{\mathrm{ref}} \right) = \frac{1}{v_{\mathrm{ref}}} \int_{s_{\mathrm{ref}}} \dot{\mathbf{x}} \otimes \mathbf{d}s_{\mathrm{ref}}, \tag{32}$$

where $\dot{\mathbf{x}}(\mathbf{X}, t) = \frac{\mathrm{d}}{\mathrm{d}t}(x^{a}\mathbf{g}_{a})$ is a compatible (material) surface velocity. Consider the following equality [72]:

$$\frac{1}{v_{\mathrm{ref}}} \int_{v_{\mathrm{ref}}} \dot{\mathbf{f}}\mathbf{s}\, \mathrm{d}v_{\mathrm{ref}} - \dot{\mathbf{F}}\mathbf{S} = \frac{1}{v_{\mathrm{ref}}} \int_{s_{\mathrm{ref}}} (\dot{\mathbf{x}} - \dot{\mathbf{F}}\mathbf{X}) \otimes (\mathbf{n}_{\mathbf{ref}}(\mathbf{s} - \mathbf{S}))\, \mathrm{d}s_{\mathrm{ref}}. \tag{33}$$

The right-hand side of Eq. (33) is zero for linear displacement, constant traction, and certain periodic boundary conditions specified with respect to the reference configuration. Assuming

henceforward such boundary conditions apply as representative for our crystal element, the volume-averaged stress work rate per unit volume is found as

$$\frac{1}{v_{\text{ref}}}\int_{s_{\text{ref}}} t^a g_{ab}\dot{x}^b \,\mathrm{d}s_{\text{ref}} = \frac{1}{v_{\text{ref}}}\int_{v_{\text{ref}}} S^{Aa} g_{ab}\dot{f}^b_{\cdot A}\,\mathrm{d}v_{\text{ref}} = S^A_{\cdot a}\dot{F}^a_{\cdot A}, \tag{34}$$

where we have used Gauss's theorem in $(34)_1$.

The balance of energy for a purely mechanical process, considering the localized form of (34) in the absence of heat flux due to conduction or internal heat supply, is written as

$$\dot{u}_0 = S^A_{\cdot a}\dot{f}^a_{\cdot A}, \tag{35}$$

with u_0 the local internal energy *per unit volume* in the reference configuration. The corresponding averaged energy balance then follows from Eq. $(34)_2$ and (35) as

$$\dot{U}_0 = S^A_{\cdot a}\dot{F}^a_{\cdot A}, \tag{36}$$

where $U_0 \equiv (v_{\text{ref}})^{-1}\int_{v_{\text{ref}}} u_0 \mathrm{d}v_{\text{ref}}$ is the average internal energy per unit reference configuration volume. Notice that Eqs. (35) and (36) are constitutive assumptions, prohibiting conjugate microstresses to second-order gradients of deformation from performing mechanical work on the external boundaries of $\mathrm{d}v_{\text{ref}}$ and v_{ref}, respectively. These rather strong assumptions are in agreement with previous treatments by Teodosiu [3], Steinmann [32], Acharya and Bassani [33,73], Menzel and Steinmann [9], Bammann [34], Bassani [74], and Regueiro et al. [39]. On the other hand, they are contradictory to the models of Teodosiu [1], Dillon and Kratochvil [5], Naghdi and Srinivasa [38,28], Le and Stumpf [30,31], Shizawa and Zbib [16,17], and Gurtin [13,36].

Introducing η_0 as the average specific entropy per unit reference volume, the Clausius–Duhem inequality is written

$$\dot{\eta}_0 \geqslant 0, \tag{37}$$

again in the absence of heat flux due to conduction or internal heat supply. The average Helmholtz free energy per unit volume in the reference configuration, ψ_0, is then defined by

$$\psi_0 \equiv U_0 - \eta_0\theta, \tag{38}$$

with θ the absolute temperature. Substituting Eqs. (36) and (38) into the Clausius–Duhem inequality (37) and assuming stationary temperature then yields a reduced form for the entropy inequality:

$$S^A_{\cdot a}\dot{F}^a_{\cdot A} \geqslant \dot{\psi}_0. \tag{39}$$

The remaining balance laws at the level of the volume element are now presented:

$$\rho_0 = \rho J, \quad S^{Aa}_{|A} = 0, \quad F^a_{\cdot A}S^{Ab} = S^{Aa}F^b_{\cdot A}. \tag{40}$$

Eq. $(40)_1$ provides the usual relationship between current, ρ, and reference, ρ_0, average mass densities. Eq. $(40)_2$ and $(40)_3$ follow from volume averaging the microscopic balance laws in Eq. (29) and by assuming that boundary conditions imposed on the crystal volume element are such that the right-hand side of Eq. (33) is zero throughout the deformation process. The last of (40) leads to symmetry of the Cauchy stress $\boldsymbol{\Sigma}$, as defined in Eq. (31).

Notice that inequality (39) is written in terms of two-point tensors $\mathbf{S}$ and $\mathbf{F}$ and the free energy per unit reference volume ψ_0. We shall later find it useful to express (39) in terms of quantities with all components referred to intermediate configuration $\tilde{b}_{\text{int}}$ (i.e., the relaxed intermediate configuration of elastoplasticity), which we view as the most convenient configuration for deducing thermodynamic restrictions and posing constitutive assumptions (see also [16,17,39]). Expression of (39) in the intermediate configuration is achieved here by first mapping to the current configuration, then pulling back by the two-point elastic deformation gradient $\mathbf{F}^{\text{e}}$. From (31) we have

$$S^{A}_{\cdot a}\dot{F}^{a}_{\cdot A} = J\Sigma^{ab}\underbrace{g_{bc}\dot{F}^{c}_{\cdot A}F^{-1}_{\cdot a}A}_{\equiv L_{ba}} = J\Sigma^{ab}L_{ba}, \tag{41}$$

with $\mathbf{L}$ the spatial velocity gradient. Substituting into (39) and multiplying by the inverse of the Jacobian invariant $\widetilde{J} \equiv \det\widetilde{\mathbf{F}}\sqrt{\tilde{g}/G} > 0$ then gives the Clausius–Duhem inequality in the current configuration, i.e.

$$(\Sigma^{ab}L_{ba} + \psi_0\dot{J}^{-1}) \geqslant \dot{\psi}, \tag{42}$$

where the free energy per unit current volume is $\psi \equiv J^{-1}\psi_0$. From the symmetry of $\boldsymbol{\Sigma}$ and $\mathbf{g}^{-1}$, and using the standard identities $\overline{J^{-1}J} = 0$ and $\dot{J} = Jg^{ab}L_{ba}$, Eq. (42) can be simplified to read

$$\langle(\boldsymbol{\Sigma} - \psi\mathbf{g}^{-1}), \mathscr{L}_{\mathbf{v}}(\mathbf{g})\rangle \geqslant 2\dot{\psi}, \tag{43}$$

with $\mathscr{L}_{\mathbf{v}}$ the Lie derivative with respect to the spatial velocity field $\mathbf{v} = \dot{\mathbf{x}} \circ \boldsymbol{\varphi}^{-1}$, and with $\langle\mathbf{A},\mathbf{B}\rangle = \text{tr}(\mathbf{AB})$ the dual product defined for second-rank tensors $\mathbf{A}$ and $\mathbf{B}$. We next define the velocity gradient $\widetilde{\mathbf{L}}$ referred to intermediate configuration $\tilde{b}_{\text{int}}$ as

$$\widetilde{L}^{\alpha}_{\cdot\beta} \equiv F^{\text{e}-1^{\alpha}}_{\cdot a}L^{a}_{\cdot b}F^{\text{e}^{b}}_{\cdot\beta} \tag{44}$$

and we define the mixed-variant elastic second Piola–Kirchhoff stress $\widetilde{\mathbf{S}}$ and the Mandel stress [75] $\widetilde{\mathbf{M}}$ as

$$\widetilde{S}^{\alpha}_{\cdot\beta} \equiv J^{\text{e}}F^{\text{e}-1^{\alpha}}_{\cdot a}\Sigma^{ac}g_{cb}F^{\text{e}-\text{T}^{b}}_{\cdot\beta}, \quad \widetilde{M}^{\alpha}_{\cdot\beta} \equiv J^{\text{e}}F^{\text{e}\text{T}^{\alpha}}_{\cdot a}\Sigma^{ac}g_{cb}F^{e-\text{T}^{b}}_{\cdot\beta} = \widetilde{C}^{\text{e}^{\alpha}}_{\cdot\chi}\widetilde{S}^{\chi}_{\cdot\beta}, \tag{45}$$

where $\widetilde{C}^{\text{e}\alpha}_{\cdot\chi} \equiv \tilde{g}^{\alpha\beta}F^{\text{e}a}_{\cdot\chi}g_{ab}F^{\text{e}b}_{\cdot\beta}$ and $J^{\text{e}} \equiv \det\mathbf{F}^{\text{e}}\sqrt{g/\tilde{g}}$. Then from relations (39), (41) and $(45)_2$, we can obtain

$$\widetilde{J}\widetilde{L}^{\alpha}_{\cdot\beta}\widetilde{M}^{\text{T}^{\beta}}_{\cdot\alpha} \geqslant \dot{\psi}_0. \tag{46}$$

Multiplying (46) by $\widetilde{J}^{-1} > 0$ and using the relation $\dot{\overline{\widetilde{J}^{-1}}} = -\widetilde{J}^{-2}\dot{\widetilde{J}} = -\widetilde{J}^{-1}\dot{\widetilde{F}}^{\alpha}_{\cdot A}\widetilde{F}^{-1^{A}}_{\cdot\alpha}$, along with $\widetilde{\psi} \equiv \widetilde{J}^{-1}\psi_0$, then gives

$$\widetilde{L}^{\alpha}_{\cdot\beta}\widetilde{M}^{\mathrm{T}^{\beta}}_{\cdot\alpha} - \widetilde{\psi}\dot{\widetilde{F}}^{\alpha}_{\cdot A}\widetilde{F}^{-1^{A}}_{\cdot\alpha} \geqslant \dot{\widetilde{\psi}}, \tag{47}$$

which is the reduced entropy inequality mapped to configuration $\tilde{b}_{\mathrm{int}}$, with energetic quantities defined on a per-unit-volume basis with respect to local element volume $\tilde{v}_{\mathrm{int}}$.

4. Crystal plasticity model

Hereafter we more fully develop a continuum crystal plasticity model, focusing on a formulation couched at a single length scale ℓ_{ref} rather than one phrased in terms of volume averages. This is necessary for typical numerical implementations, wherein each volume element v_{ref} corresponds to the local region about an integration point in a finite element simulation, for example. The microscopic deformation gradients $\mathbf{f}$, $\tilde{\mathbf{f}}$, $\mathbf{f}^{\mathrm{e}}$, $\mathbf{f}^{\mathrm{p}}$, $\tilde{\mathbf{f}}^{\mathrm{e}}$, $\tilde{\mathbf{f}}^{\mathrm{p}}$, and $\mathbf{f}^{\mathrm{c}}$ were introduced in Section 2 for illustrative purposes and are not calculated explicitly in this model. The same can be said for the microscopic kinetic variables—such as $\mathbf{t}$, $\mathbf{s}$ and u_0, for example—of Section 3. Instead, we consider here the evolution of the *average* deformation gradients for the crystalline volume element (e.g., $\mathbf{F}$, $\mathbf{F}^{\mathrm{e}}$, $\widetilde{\mathbf{F}}^{\mathrm{i}}$, and $\overline{\mathbf{F}}^{\mathrm{p}}$), the *average* stresses (e.g., $\mathbf{S}$ and $\boldsymbol{\Sigma}$), and the *average* energies (e.g., U_0 and ψ_0). Since the microscopic deformations and local lattice rearrangements within the volume element are no longer explicitly tracked, we are unable to invoke Eq. (9) to determine $\mathbf{V}^{\mathrm{e}}$, Eq. (10) for $\mathbf{R}^{\mathrm{e}}$, Eq. (15) for $\overline{\mathbf{F}}^{\mathrm{p}}$, Eq. (17) for $\widetilde{\mathbf{F}}^{\mathrm{i}}$, or Eq. (26) to calculate the local incompatibility $\tilde{\mathbf{b}}^{\mathrm{e}}$ within microscopic subregions of the crystal element. Likewise, we are unable to calculate local residual stress fields and elastic energies associated with $\tilde{\mathbf{f}}^{\mathrm{e}}$ in the model forthcoming in Section 4. Instead, we must rely upon additional constitutive assumptions and corresponding balance relations to ready our model for implementation—these are considered in detail in what follows. Of course, the constitutive assumptions we make hereafter are motivated by the physically-based, multiscale averaging treatment of Sections 2 and 3.

4.1. Kinematics, balance laws, and thermodynamics: summary

The fundamental thermomechanical relations already derived in Sections 2 and 3 and applied now to a "single-scale" crystal plasticity formulation are restated here for clarity and ease of reference.

Deformation gradient:

$$\mathbf{F} = \frac{\partial \mathbf{x}}{\partial \mathbf{X}} = \mathbf{F}^{\mathrm{e}}\underbrace{\widetilde{\mathbf{F}}^{\mathrm{i}}\overline{\mathbf{F}}^{\mathrm{p}}}_{\widetilde{\mathbf{F}}} = \underbrace{\mathbf{V}^{\mathrm{e}}\mathbf{R}^{\mathrm{e}}}_{\mathbf{F}^{\mathrm{e}}}\underbrace{\widetilde{\mathbf{V}}^{\mathrm{i}}\widetilde{\mathbf{R}}^{\mathrm{i}}}_{\widetilde{\mathbf{F}}^{\mathrm{i}}}\overline{\mathbf{F}}^{\mathrm{p}}. \tag{48}$$

Dislocation density tensor (GNDs):

$$\tilde{\mathbf{A}}^{\mathrm{e}} = J^{\mathrm{e}}\mathbf{F}^{\mathrm{e}-1}(\mathrm{curl}\mathbf{F}^{\mathrm{e}-1})^{\mathrm{T}}. \tag{49}$$

Mechanical stresses:

$$\widetilde{\mathbf{M}} = \tilde{\mathbf{g}}^{-1}\widetilde{\mathbf{C}}^{\mathrm{e}}\widetilde{\mathbf{S}} = J^{e}\mathbf{F}^{\mathrm{eT}}\boldsymbol{\Sigma}\mathbf{g}\mathbf{F}^{\mathrm{e-T}} = \widetilde{J}^{-1}\mathbf{F}^{\mathrm{eT}}\mathbf{F}\mathbf{S}\mathbf{g}\mathbf{F}^{\mathrm{e-T}}. \tag{50}$$

Mass conservation:

$$\rho_0 = \rho J. \tag{51}$$

Balance of linear momentum (quasi-static):

$$\mathrm{Div}(\mathbf{S}) = \mathbf{0}. \tag{52}$$

Balance of angular momentum (quasi-static, intermediate configuration):

$$\widetilde{\mathbf{S}} - \widetilde{\mathbf{S}}^{\mathrm{T}} = \mathbf{0}. \tag{53}$$

Balance of energy (mechanical case, intermediate configuration):

$$\langle \widetilde{\mathbf{M}}^{\mathrm{T}}, \underbrace{\mathbf{F}^{\mathrm{e}-1}\dot{\mathbf{F}}\mathbf{F}^{-1}\mathbf{F}^{\mathrm{e}}}_{\widetilde{\mathbf{L}}} \rangle = \widetilde{J}^{-1}\dot{U}_0. \tag{54}$$

Entropy inequality (mechanical case, intermediate configuration):

$$\langle \widetilde{\mathbf{M}}^{\mathrm{T}}, \widetilde{\mathbf{L}} \rangle - \langle \widetilde{\psi}\tilde{\mathbf{1}}, \dot{\widetilde{\mathbf{F}}}\widetilde{\mathbf{F}}^{-1} \rangle \geqslant \dot{\widetilde{\psi}}. \tag{55}$$

4.2. Free energy and consequences of the dissipation inequality

We make the following general assumption regarding the dependency of the Helmholtz free energy function for the crystal volume element, referred to relaxed intermediate configuration $\tilde{b}_{\mathrm{int}}$ and neglecting temperature effects:

$$\widetilde{\psi} = \widetilde{\psi}(\widetilde{\mathbf{C}}^{\mathrm{e}}, \widetilde{\mathbf{V}}^{\mathrm{i}}, \tilde{\mathbf{A}}^{\mathrm{e}}, \tilde{\varepsilon}_{\mathrm{SS}}, \tilde{\mathbf{g}}) = \widetilde{\psi}(\widetilde{C}^{\mathrm{e}}_{\alpha\beta}, \widetilde{V}^{\mathrm{i}^{\alpha}}_{\cdot\beta}, \widetilde{A}^{\mathrm{e}^{\alpha\beta}}, \tilde{\varepsilon}_{\mathrm{SS}}, \tilde{g}_{\alpha\beta}). \tag{56}$$

The covariant elastic strain tensor $\widetilde{C}^{\mathrm{e}}_{\alpha\beta} \equiv F^{\mathrm{e}a}_{\cdot\alpha} g_{ab} F^{\mathrm{e}b}_{\cdot\beta}$ is included to model the change in average energy with a change in external loads, a standard assumption in finite crystalline elastoplasticity theories (cf. [76]). The left stretch tensor derived from $\widetilde{\mathbf{F}}^{\mathrm{i}}$, denoted by $\widetilde{\mathbf{V}}^{\mathrm{i}}$, is included to reflect the contribution to the free energy from residual microelasticity within the volume element, and is non-negligible when the deformation within the volume element is heterogeneous (e.g., during grain subdivision). Kratochvil [77] and Lion [78] made similar constitutive assumptions. The elastic energy due to the average elastic curvature in the volume element attributed to GNDs is reflected by the inclusion of $\tilde{\mathbf{A}}^{\mathrm{e}}$, a particular assumption also suggested explicitly by Bammann [34], Gurtin [36], and Regueiro et al. [39]. Since the GND density tensor does not include a

measure of the total length of all dislocation lines (e.g., SSDs consisting of closed dislocation loops and dislocation lines of opposing signs), the scalar parameter $\tilde{\varepsilon}_{\mathrm{SS}} \equiv \tilde{b}\sqrt{\tilde{\rho}_{\mathrm{SS}}}$ is included to model the net contribution of the elastic self-energy of the SSDs to the total free energy (cf. [79,80]). The scalar norm of the Burgers vector (e.g., the lattice parameter) is denoted by $\tilde{b}$, while the line length of SSDs per unit intermediate configuration volume is written $\tilde{\rho}_{\mathrm{SS}}$. We regard $\tilde{\varepsilon}_{\mathrm{SS}}$ as a local residual lattice strain measure due to the presence of SSDs [34].

It is emphasized that all independent variables in the free energy function are "elastic" variables, in contradiction to works of Naghdi and Srinivasa [38,28], Gurtin [13], and Svendsen [37], among others, who include a dependency upon the plastic deformation gradient and/or higher gradients of plastic deformation. We treat the plastic deformation gradient $\widetilde{\mathbf{F}}^{\mathrm{p}}$ as a continuum idealization of the rigid sliding of portions of the lattice due to relative motion of elastic blocks of material contained between slip planes. Such motions clearly do not alter the energetic properties of material within the blocks, and therefore should not influence the Helmholtz free energy. Reasoning behind inclusion of the metric $\tilde{\mathbf{g}}$ will be explained later.

Notice that each of the constitutive variables in (56) is invariant with respect to superposed rigid body motions in the current configuration: $\mathbf{x} \to \mathbf{Q}\mathbf{x} + \mathbf{c}$, with $\mathbf{Q} \in \mathrm{SO}_3$ a rigid body rotation matrix and $\mathbf{c}$ a constant translation vector:

$$\begin{aligned}
&\mathbf{F}^{\mathrm{e}} \to \mathbf{Q}\mathbf{F}^{\mathrm{e}} \Rightarrow \widetilde{\mathbf{C}}^{\mathrm{e}} \to \widetilde{\mathbf{C}}^{\mathrm{e}}, \quad \widetilde{\mathbf{F}}^{\mathrm{i}} \to \widetilde{\mathbf{F}}^{\mathrm{i}} \Rightarrow \widetilde{\mathbf{V}}^{\mathrm{i}} \to \widetilde{\mathbf{V}}^{\mathrm{i}}, \\
&\tilde{\mathbf{A}}^{\mathrm{e}} = J^{\mathrm{e}}\mathbf{F}^{\mathrm{e}-1}(\mathrm{curl}\mathbf{F}^{\mathrm{e}-1})^{\mathrm{T}} \to J^{\mathrm{e}}(\det\mathbf{Q})\mathbf{F}^{\mathrm{e}-1}\mathbf{Q}^{\mathrm{T}}(\mathrm{curl}(\mathbf{F}^{\mathrm{e}-1}\mathbf{Q}^{\mathrm{T}}))^{\mathrm{T}} = \tilde{\mathbf{A}}^{\mathrm{e}}, \\
&\tilde{\rho}_{\mathrm{SS}} \to \tilde{\rho}_{\mathrm{SS}} \Rightarrow \tilde{\varepsilon}_{\mathrm{SS}} \to \tilde{\varepsilon}_{\mathrm{SS}}, \quad \tilde{\mathbf{g}} \to \tilde{\mathbf{g}}.
\end{aligned} \tag{57}$$

Even though $\widetilde{\mathbf{F}}^{\mathrm{i}}$ is unaffected by rigid transformations of the current configuration [77], we choose not to include the rotational part of $\widetilde{\mathbf{F}}^{\mathrm{i}}$, denoted by $\widetilde{\mathbf{R}}^{\mathrm{i}}$, in the free energy function because rigid-body rotations of the volume element in the unloaded configuration $\tilde{b}_{\mathrm{int}}$ do not influence the stored elastic energy.

We define the conjugate stresses to the independent state variables included in (56):

$$\widetilde{\mathbf{S}}^{\mathrm{e}} \equiv \frac{\partial\widetilde{\psi}}{\partial\widetilde{\mathbf{C}}^{\mathrm{e}}}, \quad \widetilde{\mathbf{S}}^{\mathrm{i}} \equiv \frac{\partial\widetilde{\psi}}{\partial\widetilde{\mathbf{V}}^{\mathrm{i}}}, \quad \widetilde{\mathbf{S}}^{\mathrm{GN}} \equiv \frac{\partial\widetilde{\psi}}{\partial\tilde{\mathbf{A}}^{\mathrm{e}}}, \quad \widetilde{S}^{\mathrm{SS}} \equiv \frac{\partial\widetilde{\psi}}{\partial\tilde{\varepsilon}_{\mathrm{SS}}}, \quad \widetilde{\mathbf{S}}^{\mathrm{g}} \equiv \frac{\partial\widetilde{\psi}}{\partial\tilde{\mathbf{g}}}. \tag{58}$$

Notice that $\widetilde{\mathbf{S}}^{\mathrm{GN}}$ is a couple stress, with units of *force/length*, while the remaining stress measures, $\widetilde{\mathbf{S}}^{\mathrm{e}}$, $\widetilde{\mathbf{S}}^{\mathrm{i}}$, $\widetilde{S}^{\mathrm{SS}}$, and $\widetilde{\mathbf{S}}^{\mathrm{g}}$ possess the standard stress dimensions of *force/length*^{2}. Expanding $\widetilde{\psi}$ in (55) using the definitions of (58) gives

$$\widetilde{L}^{\alpha}_{\cdot\beta}\widetilde{M}^{\mathrm{T}\beta}_{\cdot\alpha} - \dot{\widetilde{\psi}} \geqslant \widetilde{S}^{\mathrm{e}\alpha\beta}\dot{\widetilde{C}}^{\mathrm{e}}_{\alpha\beta} + \widetilde{S}^{\mathrm{i}^{*\beta}}_{\cdot\alpha}\dot{\widetilde{V}}^{\mathrm{i}^{\alpha}}_{\cdot\beta} + \widetilde{S}^{\mathrm{GN}}_{\alpha\beta}\dot{\tilde{A}}^{\mathrm{e}\alpha\beta} + \widetilde{S}^{\mathrm{SS}}\dot{\tilde{\varepsilon}}_{\mathrm{SS}} + \widetilde{S}^{\mathrm{g}\alpha\beta}\dot{\tilde{g}}_{\alpha\beta}, \tag{59}$$

where the dual map [81,82] is denoted by $()^*$ and satisfies $(A^a_{\cdot b})^* = A^{*\cdot a}_{b}$. From the three-term multiplicative decomposition of the deformation gradient, $\mathbf{F} = \mathbf{F}^{\mathrm{e}}\widetilde{\mathbf{F}}^{\mathrm{i}}\overline{\mathbf{F}}^{\mathrm{p}}$, of Eqs. (16) and (48), the velocity gradient in the intermediate configuration, $\widetilde{\mathbf{L}}$, can be partitioned as

$$\widetilde{\mathbf{L}} \equiv \mathbf{F}^{\mathrm{e}-1}\underbrace{\dot{\mathbf{F}}\mathbf{F}^{-1}}_{\mathbf{L}}\mathbf{F}^{\mathrm{e}} = \underbrace{\mathbf{F}^{\mathrm{e}-1}\dot{\mathbf{F}}^{\mathrm{e}}}_{\widetilde{\mathbf{L}}^{\mathrm{e}}} + \underbrace{\dot{\widetilde{\mathbf{F}}}^{\mathrm{i}}\widetilde{\mathbf{F}}^{\mathrm{i}-1}}_{\widetilde{\mathbf{L}}^{\mathrm{i}}} + \underbrace{\widetilde{\mathbf{F}}^{\mathrm{i}}\dot{\overline{\mathbf{F}}}^{\mathrm{p}}\overline{\mathbf{F}}^{\mathrm{p}-1}\widetilde{\mathbf{F}}^{\mathrm{i}-1}}_{\widetilde{\mathbf{L}}^{\mathrm{p}}}. \tag{60}$$

Further algebraic manipulations give

$$\langle\widetilde{\mathbf{L}},\widetilde{\mathbf{M}}^{\mathrm{T}}\rangle = \left\langle\widetilde{\mathbf{S}}\tilde{\mathbf{g}}^{-1},\frac{1}{2}\dot{\widetilde{\mathbf{C}}}^{\mathrm{e}}\right\rangle + \langle\widetilde{\mathbf{M}}^{\mathrm{T}},\widetilde{\mathbf{L}}^{\mathrm{i}}+\widetilde{\mathbf{L}}^{\mathrm{p}}\rangle, \quad \underbrace{\dot{\widetilde{\mathbf{F}}}^{\mathrm{i}}\widetilde{\mathbf{F}}^{\mathrm{i}-1}}_{\widetilde{\mathbf{L}}^{\mathrm{i}}} = \dot{\widetilde{\mathbf{V}}}^{\mathrm{i}}\widetilde{\mathbf{V}}^{\mathrm{i}-1} + \widetilde{\mathbf{V}}^{\mathrm{i}}\underbrace{\dot{\widetilde{\mathbf{R}}}^{\mathrm{i}}\widetilde{\mathbf{R}}^{\mathrm{i}\mathrm{T}}}_{\widetilde{\mathbf{W}}^{\mathrm{i}}}\widetilde{\mathbf{V}}^{\mathrm{i}-1}, \tag{61}$$

where the spin $\widetilde{\mathbf{W}}^{\mathrm{i}}$ is skew via $\tilde{g}_{\alpha\beta}\widetilde{W}^{i\beta}_{\cdot\chi} = -\tilde{g}_{\chi\beta}\widetilde{W}^{i\beta}_{\cdot\alpha}$. Using Eqs. (60) and (61) in inequality (59) then results in

$$\begin{aligned}&\left(\frac{1}{2}\widetilde{S}^{\alpha}_{\cdot\chi}\tilde{g}^{-1\chi\beta} - \widetilde{S}^{\mathrm{e}\alpha\beta}\right)\dot{\widetilde{C}}^{\mathrm{e}}_{\alpha\beta} + ((\widetilde{M}^{\mathrm{T}\beta}_{\cdot\chi} - \widetilde{\psi}\delta^{\beta}_{\cdot\chi})\widetilde{V}^{\mathrm{i}-1\chi}_{\cdot\alpha} - \widetilde{S}^{\mathrm{i}*\beta}_{\cdot\alpha})\dot{\widetilde{V}}^{\mathrm{i}^{\alpha}}_{\cdot\beta} - \widetilde{S}^{g\alpha\beta}\dot{\tilde{g}}_{\alpha\beta}\\ &\quad + (\widetilde{V}^{\mathrm{i}^{\beta}}_{\cdot\chi}\widetilde{M}^{\mathrm{T}\chi}_{\cdot\gamma}\widetilde{V}^{\mathrm{i}-1\gamma}_{\cdot\alpha})\widetilde{W}^{\mathrm{i}^{\alpha}}_{\cdot\beta} - \widetilde{S}^{\mathrm{GN}}_{\alpha\beta}\dot{\widetilde{A}}^{\mathrm{e}^{\alpha\beta}} - \widetilde{S}^{\mathrm{SS}}\dot{\tilde{\varepsilon}}_{\mathrm{SS}} + (\widetilde{M}^{\mathrm{T}\beta}_{\cdot\alpha} - \widetilde{\psi}\delta^{\beta}_{\cdot\alpha})\tilde{L}^{\mathrm{p}^{\alpha}}_{\cdot\beta} \geqslant 0.\end{aligned} \tag{62}$$

Assuming that (62) must hold for independent specification of the elastic strain rate and the other rate variables [83,84] we arrive at standard relationships between the (mechanical) elastic stresses $\widetilde{\mathbf{S}}$, $\boldsymbol{\Sigma}$, $\mathbf{S}$, and $\mathbf{T}$, and the lattice stress $\widetilde{\mathbf{S}}^{\mathrm{e}}$ conjugate to $\widetilde{\mathbf{C}}^{\mathrm{e}}$

$$2\widetilde{\mathbf{S}}^{\mathrm{e}} = 2\frac{\partial\widetilde{\psi}}{\partial\widetilde{\mathbf{C}}^{\mathrm{e}}} = \widetilde{\mathbf{S}}\tilde{\mathbf{g}}^{-1} = J^{\mathrm{e}}\mathbf{F}^{\mathrm{e}-1}\boldsymbol{\Sigma}\mathbf{F}^{\mathrm{e}-*} = \widetilde{J}^{-1}\widetilde{\mathbf{F}}\mathbf{S}\mathbf{F}^{\mathrm{e}-*} = \widetilde{J}^{-1}\mathbf{F}^{\mathrm{e}-1}\mathbf{T}\widetilde{\mathbf{F}}^{*}, \tag{63}$$

where $\mathbf{T} \equiv \mathbf{S}^{\mathrm{T}}$ is the contravariant first Piola–Kirchhoff stress tensor, and the final equality follows from $(40)_3$. More familiar and compact constitutive equations for the Cauchy stress and first Piola–Kirchhoff stress are then derived readily with the chain rule of differentiation

$$\Sigma^{ab} = 2J^{\mathrm{e}-1}\frac{\partial\widetilde{\psi}}{\partial\widetilde{C}^{\mathrm{e}}_{\alpha\beta}}\underbrace{F^{\mathrm{e}^{a}}_{\cdot\alpha}F^{\mathrm{e}^{b}}_{\cdot\beta}}_{=\partial\widetilde{C}^{\mathrm{e}}_{\alpha\beta}/\partial g_{ab}} = 2J^{e-1}\frac{\partial\widetilde{\psi}}{\partial g_{ab}} \approx 2\frac{\partial\psi}{\partial g_{ab}}, \tag{64}$$

$$T^{aA} = 2\widetilde{J}F^{-1^{A}}_{\cdot b}F^{\mathrm{e}^{b}}_{\cdot\alpha}\frac{\partial\widetilde{\psi}}{\partial\widetilde{C}^{\mathrm{e}}_{\alpha\beta}}F^{\mathrm{e}^{a}}_{\cdot\beta} = \underbrace{\widetilde{J}\,\widetilde{F}^{-1^{A}}_{\cdot\alpha}\frac{\partial\tilde{\psi}}{\partial F^{\mathrm{e}^{c}}_{\cdot\alpha}}}_{=\partial\widetilde{\psi}/\partial F^{\mathrm{c}}_{\cdot A}}g^{ca} = \widetilde{J}\frac{\partial\widetilde{\psi}}{\partial F^{\mathrm{c}}_{\cdot A}}g^{ca} \approx \frac{\partial\psi_0}{\partial F^{\mathrm{c}}_{\cdot A}}g^{ca}. \tag{65}$$

The final equality in (64) is rigorous only when $\partial J^{\mathrm{e}-1}/\partial\mathbf{g} = \mathbf{0}$ (e.g., Cartesian current coordinates), while the final equality in (65) is ensured only when $\partial\widetilde{J}/\partial\mathbf{F} = \mathbf{0}$ (e.g., when the total inelastic deformation is isochoric). We next define (cf. [85])

$$\widetilde{\mathbf{P}} \equiv \widetilde{\mathbf{M}}^{\mathrm{T}} - \widetilde{\psi}\tilde{\mathbf{1}} = J^{\mathrm{e}}\mathbf{F}^{\mathrm{e}-1}\underbrace{(\boldsymbol{\Sigma}\mathbf{g} - \psi\mathbf{1})}_{\mathbf{p}}\mathbf{F}^{\mathrm{e}} = \widetilde{J}^{-1}\widetilde{\mathbf{F}}\underbrace{(\mathbf{F}^{\mathrm{T}}\mathbf{T}\mathbf{G} - \psi_0\mathbf{1}_0)}_{\mathbf{P}}\widetilde{\mathbf{F}}^{-1} \tag{66}$$

as the push-forward of the mixed-variant reference configuration Eshelby [1] [86] energy–momentum tensor $\mathbf{P}$, or equivalently as the pull-back of the current configuration Eshelby stress tensor $\mathbf{p}$. In Eq. (66), $\mathbf{1}_0$, $\tilde{\mathbf{1}}$, and $\mathbf{1}$ denote mixed-variant identity maps on configurations b_{ref}, $\tilde{b}_{\mathrm{int}}$, and b_{cur}, respectively. Upon substituting (63) and (66) into (62) and assuming that $\dot{\tilde{\mathbf{g}}} = \mathbf{0}$, we arrive at a reduced form of the dissipation inequality:

$$\langle\widetilde{\mathbf{P}}\widetilde{\mathbf{V}}^{\mathrm{i}-1} - \widetilde{\mathbf{S}}^{\mathrm{i}*}, \dot{\widetilde{\mathbf{V}}}^{\mathrm{i}} + \langle\widetilde{\mathbf{V}}^{\mathrm{i}}\widetilde{\mathbf{P}}\widetilde{\mathbf{V}}^{\mathrm{i}-1}, \widetilde{\mathbf{W}}^{\mathrm{i}}\rangle - \langle\widetilde{\mathbf{S}}^{\mathrm{GNT}}, \dot{\tilde{\mathbf{A}}}^{e}\rangle - \langle\widetilde{S}^{\mathrm{SS}}, \dot{\tilde{\varepsilon}}_{\mathrm{SS}}\rangle + \langle\widetilde{\mathbf{P}}, \widetilde{\mathbf{D}}^{\mathrm{p}} + \widetilde{\mathbf{W}}^{\mathrm{p}}\rangle \geqslant 0. \tag{67}$$

Notice that both the plastic deformation rate $\widetilde{D}^{\mathrm{p}^{\alpha}}_{\cdot\beta} \equiv \tilde{g}^{\alpha\delta}(\tilde{\mathbf{g}}\widetilde{\mathbf{L}}^{\mathrm{p}})_{(\delta\beta)}$ and the plastic spin $\widetilde{W}^{\mathrm{p}^{\alpha}}_{\cdot\beta} \equiv \tilde{g}^{\alpha\delta}(\tilde{\mathbf{g}}\widetilde{\mathbf{L}}^{\mathrm{p}})_{[\delta\beta]}$ contribute to the dissipation, as does the spin associated with residual elasticity/subdivision $\widetilde{\mathbf{W}}^{\mathrm{i}}$. Note also the prominent role of the Eshelby stress tensor $\widetilde{\mathbf{P}}$ as a force conjugate in the plastic dissipation term (see also [85,87]).

4.3. Constitutive model

A more explicit form of the strictly mechanical, intermediate configuration free energy function (56) is now proposed on physical grounds:

$$\widetilde{\psi} = \frac{1}{2}\langle\widetilde{\mathbf{E}}^{\mathrm{e}}, (\widetilde{\mathbf{C}}^{\mathrm{eff}}(\widetilde{\mathbf{E}}^{\mathrm{i}})) : \widetilde{\mathbf{E}}^{\mathrm{e}}\rangle + c_1\mu\langle\widetilde{\mathbf{E}}^{\mathrm{i}}, \widetilde{\mathbf{E}}^{\mathrm{e}}\rangle + c_2\mu\sqrt{\langle\widetilde{\mathbf{E}}^{\mathrm{i}}, \widetilde{\mathbf{E}}^{\mathrm{i}}\rangle} + c_3\mu(\tilde{\varepsilon}_{\mathrm{SS}})^2 + \beta_{\mathrm{GN}}\mu\langle\tilde{\mathbf{A}}^{\mathrm{e}}_{\#}, \tilde{\mathbf{A}}^{\mathrm{e}}_{\#}\rangle. \tag{68}$$

The strains $\widetilde{\mathbf{E}}^{\mathrm{e}}$ and $\widetilde{\mathbf{E}}^{\mathrm{i}}$ follow from the decomposition of the total strain tensor $\widetilde{\mathbf{E}}$ referred to $\tilde{b}_{\mathrm{int}}$:

$$\widetilde{\mathbf{E}} \equiv \frac{1}{2}\widetilde{\mathbf{F}}^{-\mathrm{T}}(\mathbf{F}^{\mathrm{T}}\mathbf{F} - \mathbf{1}_0)\widetilde{\mathbf{F}}^{-1} = \widetilde{\mathbf{E}}^{\mathrm{e}} + \widetilde{\mathbf{E}}^{\mathrm{i}} + \widetilde{\mathbf{E}}^{\mathrm{p}}, \tag{69}$$

where the elastic ($\widetilde{\mathbf{E}}^{\mathrm{e}}$), heterogeneity ($\widetilde{\mathbf{E}}^{\mathrm{i}}$), and plastic ($\widetilde{\mathbf{E}}^{\mathrm{p}}$) parts are given by

$$\widetilde{\mathbf{E}}^{\mathrm{e}} \equiv \frac{1}{2}(\tilde{\mathbf{g}}^{-1}\widetilde{\mathbf{C}}^{\mathrm{e}} - \tilde{\mathbf{1}}), \quad \widetilde{\mathbf{E}}^{\mathrm{i}} \equiv \frac{1}{2}(\tilde{\mathbf{1}} - \widetilde{\mathbf{V}}^{\mathrm{i}-\mathrm{T}}\widetilde{\mathbf{V}}^{\mathrm{i}-1}), \quad \widetilde{\mathbf{E}}^{\mathrm{p}} \equiv \frac{1}{2}\widetilde{\mathbf{F}}^{\mathrm{i}-\mathrm{T}}(\tilde{\mathbf{1}} - \overline{\mathbf{F}}^{\mathrm{p}-\mathrm{T}}\overline{\mathbf{F}}^{\mathrm{p}-1})\widetilde{\mathbf{F}}^{\mathrm{i}-1}. \tag{70}$$

Notice that $\widetilde{\mathbf{E}}^{\mathrm{e}}$ and $\widetilde{\mathbf{E}}^{\mathrm{i}}$ are functions of $\widetilde{\mathbf{C}}^{\mathrm{e}}$ and $\widetilde{\mathbf{V}}^{\mathrm{i}}$, respectively, in agreement with the general form for the free energy in proposition (56). The mixed-variant GND variable $\tilde{\mathbf{A}}^{\mathrm{e}}_{\#}$ is defined as

$$\tilde{\mathbf{A}}^{\mathrm{e}}_{\#} \equiv \tilde{\mathbf{A}}^{\mathrm{e}}\tilde{\mathbf{g}}. \tag{71}$$

[1] Eshelby [86] in fact used the negative of our $\mathbf{P}$ as the referential energy–momentum tensor, with the material gradient of displacement in place of the deformation gradient. We follow here for convenience the definition and sign convention of Le and Stumpf [87] and Le et al. [76].

Components of the fourth-rank effective elastic modulus tensor for the volume element in the intermediate configuration are denoted by $(\widetilde{C}^{\text{eff}})^{\alpha\cdot\cdot\chi}_{\cdot\beta\delta\cdot}$, and μ is a characteristic elastic constant for a perfect reference lattice (e.g., an average reference shear modulus). Finally, c_1, c_2, and c_3 are dimensionless scalar constants, and β_{GN} is a (possibly) evolving scalar parameter that will be addressed more later (Eqs. (72) and (73)), with dimensions of *length*^{2}. Notice the role of $\tilde{\mathbf{g}}$ in defining the mixed-variant tensors $\widetilde{\mathbf{E}}^{\text{e}}$ and $\tilde{\mathbf{A}}^{\text{e}}_{\#}$, rendering its inclusion in the general free energy function (56) a necessity [87].

We now discuss the physical reasoning behind our choice of each term in the specific free energy function (68). The first term, $\frac{1}{2}\langle\widetilde{\mathbf{E}}^{\text{e}}, (\widetilde{\mathbf{C}}^{\text{eff}}(\widetilde{\mathbf{E}}^{\text{i}})) : \widetilde{\mathbf{E}}^{\text{e}}\rangle$, is reminiscent of the quadratic form seen in finite linear hyperelasticity, differing only in the sense that the effective elastic modulus tensor for the volume element, referred here to the intermediate configuration $\tilde{b}_{\text{int}}$, is assumed to depend explicitly upon $\widetilde{\mathbf{E}}^{\text{i}}$. This assumption is intended to reflect the influence of local microelastic rotations which arise, quite possibly, from grain subdivision and intragranular substructure development during plastic deformation (cf. Hughes et al. [43], Butler and McDowell [50]). For example, for a single crystal consisting of subgrains exhibiting a random distribution of local misorientations unrestricted in magnitude, the effective moduli will approach those of a random polycrystal (e.g., elastic isotropy in many metals).

The second term, $c_1\mu\langle\widetilde{\mathbf{E}}^{\text{i}}, \widetilde{\mathbf{E}}^{\text{e}}\rangle$, accounts for the aforementioned amplification of internal residual microstress fields (and the corresponding internal elastic energy) at flexing subgrain boundaries [59,60] with increases in the applied stress. The third term, $c_2\mu\sqrt{\langle\widetilde{\mathbf{E}}^{\text{i}}, \widetilde{\mathbf{E}}^{\text{i}}\rangle}$, represents a portion of the stored energy of cold work attributed to heterogeneous elastoplasticity within the volume element. The linear dependency of energy upon the effective "meso-incompatibility" strain $\widetilde{\mathbf{E}}^{\text{i}}$ is motivated from previous solutions obtained from computational micromechanics [88] in which low-angle and high-angle grain boundary arrangements were assigned as initial conditions to a deforming polycrystalline aggregate. Since the present model is intended for single crystals, we presume that data for low-angle grain boundary arrangements from this previous study are most applicable (Fig. 6(a)), and our form of the free energy term reflects an assumption of similitude between single crystals and polycrystals with low-angle boundaries. Thus, this term should be regarded as a rough initial approximation.

The fourth term, $\beta_{\text{GN}}\mu\langle\tilde{\mathbf{A}}^{\text{e}}_{\#}, \tilde{\mathbf{A}}^{\text{e}}_{\#}\rangle$, represents a quadratic dependency of the free energy upon the average density tensor of GNDs. Such an assumption is rather standard in gradient finite strain single- and polycrystalline elastoplasticity theories in the literature (cf. [9,32,34,37,39]), as is the linear dependence upon the total length of SSDs per unit volume, $\tilde{\rho}_{\text{SS}} = (\tilde{\varepsilon}_{\text{SS}}/\tilde{b})^2$ [34,39,37]. Additional experiments and/or numerical simulations are clearly needed to determine the parameters c_1, c_2, and c_3 for a particular material.

We remark that the parameter β_{GN} provides a squared effective "radius of non-local action" in our model (see also later Eqs. (90) and (93)). As $\beta_{\text{GN}} \to 0$, the contribution of GNDs to the free energy function becomes negligible, and the model assumes a local character. We hypothesize that $\ell_{\text{ref}} = \sqrt[3]{v_{\text{ref}}}$—the size of the representative crystal volume element (Eq. (1))—should influence the value of β_{GN} in some way. In other words, the size of the local crystal volume element over which the average dislocation density tensor $\tilde{\mathbf{A}}^{\text{e}}$ is calculated should have some effect upon the range of non-local interactions. For example, if we assume that the strength of non-locality is inversely related to scale (cf. [24]), then an obvious choice is

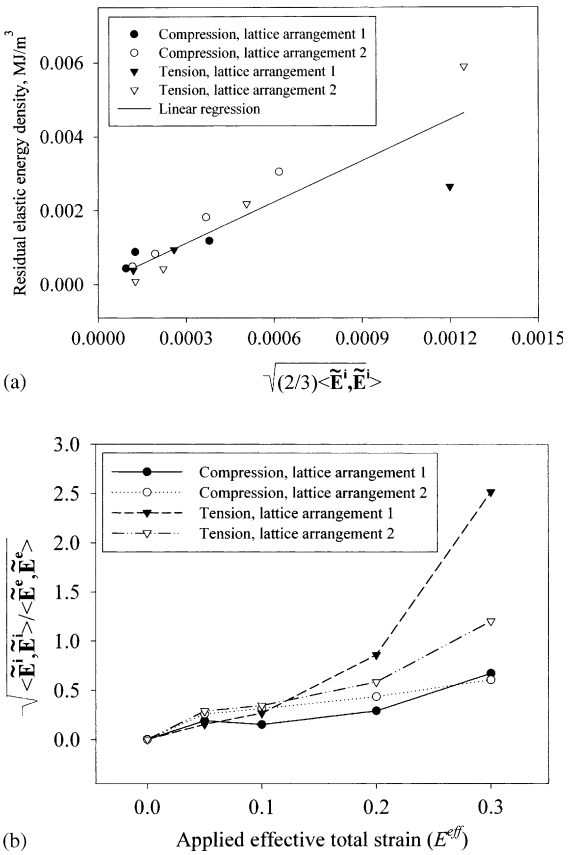

Fig. 6. Residual elastic energy versus $\sqrt{(2/3)\langle \widetilde{\mathbf{E}}^{\mathrm{i}}, \widetilde{\mathbf{E}}^{\mathrm{i}} \rangle}$ (a) and evolution of $\sqrt{\langle \widetilde{\mathbf{E}}^{\mathrm{i}}, \widetilde{\mathbf{E}}^{\mathrm{i}} \rangle / \langle \widetilde{\mathbf{E}}^{\mathrm{e}}, \widetilde{\mathbf{E}}^{\mathrm{e}} \rangle}$ versus applied effective strain (b).

$$\beta_{\mathrm{GN}} = \ell_{\mathrm{GN}}^2 \left(\frac{\ell_{\mathrm{GN}}}{\ell_{\mathrm{ref}}} \right)^{c_4}, \tag{72}$$

with ℓ_{GN} a length parameter that is characteristic for a given material (cf. [39]) and with c_4 another dimensionless material constant. In other words, if we regard ℓ_{GN} and c_4 as fixed parameters (constants) for a given material, then the non-local radius will scale with the size of the volume element according to $\ell_{\mathrm{ref}}^{-c_4/2}$. Of course, we would now need a more extensive series of tests to determine the two values ℓ_{GN} and c_4, rather than just β_{GN}. Interestingly, if we take $\ell_{\mathrm{ref}} = L_{\mathrm{G}}$, the grain size, and $c_4 = 1$, then a Hall–Petch type relation [18,19] for hardening due to GNDs is acquired via Eq. (72).

Additionally, one may argue that since the radius of non-locality should reflect a characteristic dimension of the microstructure, such as cellular structure size in ductile single crystals that subdivide (cf. [7]), then the effective length ℓ_{GN} should be an evolving, rather than stationary, parameter. In our framework, we could easily extend (72) to

$$\beta_{\mathrm{GN}} = \hat{\ell}_{\mathrm{GN}}^2 \left(\frac{\hat{\ell}_{\mathrm{GN}}}{\ell_{\mathrm{ref}}} \right)^{c_4}, \quad \hat{\ell}_{\mathrm{GN}} = \hat{\ell}_{\mathrm{GN}}(\widetilde{\mathbf{V}}^{\mathrm{i}}), \tag{73}$$

allowing the effective scaling factor $\hat{\ell}_{\mathrm{GN}}$ to evolve with the heterogeneity parameter (i.e., the grain subdivision metric) $\widetilde{\mathbf{V}}^{\mathrm{i}}$. If Eq. (73) is invoked, then the presence of $\hat{\ell}_{\mathrm{GN}}$ in the free energy function (68) will influence the values of thermodynamic force conjugates calculated via Eqs. (58) contributing to the dissipation inequality (67).

Consider a boundary value problem where $\mathbf{F}$ and its rate are prescribed incrementally as a function of time. In order to characterize completely the state of the material from the kinematic standpoint of Eq. (48), we need to specify the deformation gradient measures $\mathbf{F}^{\mathrm{e}}$, $\widetilde{\mathbf{F}}^{\mathrm{i}}$, and $\overline{\mathbf{F}}^{\mathrm{p}}$. In a hyperelastic setting (cf. [89,90]), a standard approach is to formulate evolution laws for (time rates of) $\overline{\mathbf{F}}^{\mathrm{p}}$ and $\widetilde{\mathbf{F}}^{\mathrm{i}}$, thus leaving $\mathbf{F}^{\mathrm{e}}$ to be determined from the product $\mathbf{F}(\widetilde{\mathbf{F}}^{\mathrm{i}}\overline{\mathbf{F}}^{\mathrm{p}})^{-1}$, assuming that the rate of $\mathbf{F}$ and the driving forces for each inelastic deformation measure are known at the beginning of each time increment. Such is our approach: the requisite evolution equations for $\overline{\mathbf{F}}^{\mathrm{p}}$ and $\widetilde{\mathbf{F}}^{\mathrm{i}}$ are considered next.

The time rate of *average* plastic deformation gradient in the single crystal volume element is assumed to follow from the standard kinematic framework of finite crystal plasticity [80,91–93], i.e.,

$$\dot{\overline{\mathbf{F}}}^{\mathrm{p}} = \underbrace{\left(\sum_{i=1}^{n} \dot{\gamma}^i \bar{\mathbf{s}}^i \otimes \bar{\mathbf{m}}^i \right)}_{\bar{\mathbf{L}}^{\mathrm{p}}} \overline{\mathbf{F}}^{\mathrm{p}}, \tag{74}$$

where $\dot{\gamma}^i$, $\bar{\mathbf{s}}^i$, and $\bar{\mathbf{m}}^i$ are the shearing rate, slip direction (a unit vector), and slip plane normal (a unit covector) for slip system i, all defined with respect configuration $\bar{b}_{\mathrm{p}}$ of Fig. 2. As written in (74), $\bar{\mathbf{L}}^{\mathrm{p}} \equiv \dot{\overline{\mathbf{F}}}^{\mathrm{p}}\overline{\mathbf{F}}^{\mathrm{p}-1}$ is the mixed-variant average plastic velocity gradient in configuration $\bar{b}_{\mathrm{p}}$. When the single crystalline lattice is initially heterogeneous in the reference state, or when the lattice deforms heterogeneously within the volume element, $\dot{\gamma}^i$, $\bar{\mathbf{s}}^i$, and $\bar{\mathbf{m}}^i$ are understood to be suitably-defined spatial averages of their fluctuating local counterparts. In accordance with classical crystal plasticity theory, the representation of the slip directions and slip plane normals is assumed identical in each of the unloaded configurations b_{ref} and $\bar{b}_{\mathrm{p}}$. The slip direction unit vectors and slip plane normal covectors are orthogonal in the unloaded configurations (i.e., $\langle \bar{\mathbf{m}}^i, \bar{\mathbf{s}}^i \rangle = 0$), and are typically given as initial conditions in a boundary value problem. However, their representation changes in the current configuration as a result of the elastic deformation gradient $\mathbf{F}^{\mathrm{e}}$ (cf. [76,93])

$$(s^i)^a = F^{\mathrm{e}}_{\cdot\bar{\alpha}}{}^a \delta^{\bar{\alpha}}_{\alpha} (\bar{s}^i)^{\alpha}, \quad (m^i)_a = F^{\mathrm{e}-*\cdot}_{a\alpha} \delta^{\alpha}_{\bar{\alpha}} (\bar{m}^i)_{\bar{\alpha}}. \tag{75}$$

In Eq. (75), $\mathbf{s}^i$ and $\mathbf{m}^i$ are push-forwards of their counterparts in $\bar{b}_{\mathrm{p}}$ (we have used barred Greek indices for components in $\bar{b}_{\mathrm{p}}$) and are not necessarily of unit length when the elastic stretch $\mathbf{V}^{\mathrm{e}}$ is significant, although each pair of $\mathbf{s}^i$ and $\mathbf{m}^i$ does remain orthogonal in configuration b_{cur}, as is easily verified by direct calculation. These orthogonality relations effectively prohibit dislocation climb, a non-isochoric process. Two useful consequences arise from kinematic assumption (74) and the slip plane normal-slip direction orthogonality relations. The first is

$$\dot{J}^{\mathrm{p}} = J^{\mathrm{p}}\mathrm{tr}(\bar{\mathbf{L}}^{\mathrm{p}}) = \sum_i \dot{\gamma}^i \langle \bar{\mathbf{m}}^i, \bar{\mathbf{s}}^i \rangle = 0, \tag{76}$$

meaning that the plastic flow is isochoric. The second is a reduced form of the "purely plastic" dissipation in the entropy inequality (67):

$$\langle \widetilde{\mathbf{P}}, \widetilde{\mathbf{D}}^{\mathrm{p}} + \widetilde{\mathbf{W}}^{\mathrm{p}} \rangle = \langle \underbrace{\widetilde{\mathbf{F}}^{\mathrm{i}-1}\widetilde{\mathbf{P}}\widetilde{\mathbf{F}}^{\mathrm{i}-T}}_{\overline{\mathbf{P}}}, \bar{\mathbf{L}}^{\mathrm{p}} \rangle = \langle \overline{\mathbf{P}}, \bar{\mathbf{L}}^{\mathrm{p}} \rangle = \sum_i \bar{p}^i \dot{\gamma}^i, \tag{77}$$

where $\overline{\mathbf{P}}$ is the Eshelby stress tensor mapped to "plastic" configuration $\bar{b}_{\mathrm{p}}$ and

$$\bar{p}^i \equiv \bar{P}^{\bar{\alpha}}_{\bar{\beta}} (\bar{s}^i)^{\bar{\beta}} (\bar{m}^i)_{\bar{\alpha}} \tag{78}$$

is the projected Eshelby stress on system i. We could equivalently use the pull-back of the transposed Mandel stress, $\widetilde{\mathbf{F}}^{\mathrm{i}-1}\widetilde{\mathbf{M}}^{\mathrm{T}}\widetilde{\mathbf{F}}^{\mathrm{i}-T}$, in place of $\overline{\mathbf{P}}$ in (77) and (78) since the plastic flow is volume-preserving. By assuming a particular flow potential Φ for the slip rates $\dot{\gamma}^i$, we can ensure that the dissipation in (77) is non-negative, such that the entropy inequality is satisfied automatically when the contributions of $\widetilde{\mathbf{F}}^{\mathrm{i}}$, $\tilde{\mathbf{A}}^{\mathrm{e}}$, and $\tilde{\rho}_{\mathrm{SS}}$ to the dissipation are neglected. We conveniently prescribe

$$\Phi = \sum_{i=1}^{n} \hat{\Phi}^i(\bar{p}^i, \widetilde{\mathbf{F}}^{\mathrm{i}}, \widetilde{\mathbf{S}}^{\mathrm{GN}}, \widetilde{S}^{\mathrm{SS}}) = \dot{\lambda} \sum_i \frac{\bar{\kappa}^i}{m+1} \left| \frac{\bar{p}^i}{\bar{\kappa}^i} \right|^{m+1}, \tag{79}$$

where each slip potential $\hat{\Phi}^i$ is a scalar function of its arguments. In Eq. $(79)_2$, $\dot{\lambda} > 0$ (dimensions of $1/time$) and m (dimensionless) are material parameters which we assume are constant on each slip system, while $\bar{\kappa}^i(\widetilde{\mathbf{F}}^{\mathrm{i}}, \widetilde{\mathbf{S}}^{\mathrm{GN}}, \widetilde{S}^{\mathrm{SS}}) > 0$ are scalar slip resistances (dimensions of $force/length^2$) that evolve with inelastic deformation. The slip rates are then assumed to adhere to

$$\dot{\gamma}^i = \frac{\partial \Phi}{\partial \bar{p}^i} = \frac{\partial \hat{\Phi}^i}{\partial \bar{p}^i} = \dot{\lambda}\mathrm{sgn}(\bar{p}^i) \left| \frac{\bar{p}^i}{\bar{\kappa}^i} \right|^m \quad \text{(no sum on } i\text{)}, \tag{80}$$

a power-law form reminiscent of typical flow rules proposed for classical crystal viscoplasticity [94], except that the resolved Eshelby stress is used as a conjugate variable to the slip rates in our theory. Substituting (80) into (77), we find that the purely plastic dissipation is unconditionally non-negative:

$$\sum_i \bar{p}^i \dot{\gamma}^i = \dot{\lambda} \sum_i \bar{p}^i \mathrm{sgn}(\bar{p}^i) \left| \frac{\bar{p}^i}{\bar{\kappa}^i} \right|^m \geqslant 0. \tag{81}$$

Our thermodynamic motivation for choosing the resolved Eshelby stress as a driving force for viscoplasticity is clear from (67) and (81). Our physical reasoning for selecting the Eshelby stress stems its relationship to the configurational force on a dislocation [85], as opposed to the usual resolved Cauchy stress of Schmid's law [95]. We also cite the work of Le et al. [76] who used

thermodynamic and physical arguments similar to ours to motivate usage of the Eshelby stress as a driving force for plastic deformation in a finite strain, rate-independent single crystal plasticity model.

We propose the following dependency for the positive scalar slip resistances $\bar{\kappa}^i$:

$$\bar{\kappa}^i(\widetilde{\mathbf{F}}^{\mathrm{i}}, \widetilde{\mathbf{S}}^{\mathrm{GN}}, \widetilde{S}^{\mathrm{SS}}) = \bar{\kappa}^i(\underbrace{J^{\mathrm{i}-1}\widetilde{\mathbf{F}}^{\mathrm{i}*}(\widetilde{\mathbf{S}}^{\mathrm{GN}})^{\mathrm{T}}\widetilde{\mathbf{F}}^{\mathbf{i}}}_{\bar{\mathbf{S}}^{\mathrm{GN}}}, \underbrace{\sqrt[-1]{J^{\mathrm{i}}}\widetilde{S}^{\mathrm{SS}}}_{\bar{S}^{\mathrm{SS}}}) = \bar{\kappa}^i(\bar{\mathbf{S}}^{\mathrm{GN}}, \bar{S}^{\mathrm{SS}}), \tag{82}$$

with $\bar{\mathbf{S}}^{\mathrm{GN}}$ and $\bar{S}^{\mathrm{SS}}$ complete pull-backs of $\widetilde{\mathbf{S}}^{\mathrm{GN}}$ and $\widetilde{S}^{\mathrm{SS}}$ to configuration $\bar{b}_{\mathrm{p}}$, and with $J^{\mathrm{i}} \equiv \det\widetilde{\mathbf{F}}^{\mathbf{i}}\sqrt{\det\tilde{\mathbf{g}}/\det\bar{\mathbf{g}}} > 0$ ($\bar{\mathbf{g}}$ is now introduced as a local metric on the anholonomic space $\bar{b}_{\mathrm{p}}$). The thermodynamic forces $\bar{\mathbf{S}}^{\mathrm{GN}}$ and $\bar{S}^{\mathrm{SS}}$ satisfy

$$(\bar{S}^{\mathrm{GN}})_{\bar{\alpha}\bar{\beta}} = J^{\mathrm{i}-1}\widetilde{F}^{\mathrm{i}*\cdot\alpha}_{\bar{\alpha}}\frac{\partial\widetilde{\psi}}{\partial\bar{A}^{\mathrm{e}\alpha\bar{\beta}}}\widetilde{F}^{\mathrm{i}\beta}_{\cdot\bar{\beta}} = \frac{\partial\widetilde{\psi}}{\partial\bar{A}^{\mathrm{e}\bar{\alpha}\bar{\beta}}}, \quad \bar{S}^{\mathrm{SS}} = \sqrt[-1]{J^{\mathrm{i}}}\frac{\partial\widetilde{\psi}}{\partial\tilde{\varepsilon}_{\mathrm{SS}}} = \frac{\partial\widetilde{\psi}}{\partial\bar{\varepsilon}_{\mathrm{SS}}}, \tag{83}$$

with

$$\bar{\mathbf{A}}^{\mathrm{e}} \equiv J^{\mathrm{i}}\widetilde{\mathbf{F}}^{\mathrm{i}-1}\tilde{\mathbf{A}}^{\mathrm{e}\mathrm{T}}\widetilde{\mathbf{F}}^{\mathrm{i}-*}, \quad \bar{\varepsilon}_{\mathrm{SS}} \equiv \sqrt{J^{\mathrm{i}}}\tilde{\varepsilon}_{\mathrm{SS}} \tag{84}$$

the densities of GNDs and SSDs, respectively, pulled back from $\tilde{b}_{\mathrm{int}}$ to $\bar{b}_{\mathrm{p}}$. As a more particular constitutive assumption, we represent the hardening variable for each slip system as a linear combination of the thermodynamic force conjugates to the densities of GNDs and SSDs partitioned to all systems, i.e.,

$$\bar{\kappa}^i = \bar{\kappa}^i_0 + \sqrt[-1]{\beta_{\mathrm{GN}}}h^i_{\mathrm{GN}j}\bar{S}^j_{\mathrm{GN}} + h^i_{\mathrm{SS}j}\bar{S}^j_{\mathrm{SS}}, \tag{85}$$

where $\bar{\kappa}^i_0$ is the initial friction or threshold stress for system i, $h^i_{\mathrm{GN}j}$ and $h^i_{\mathrm{SS}j}$ comprise $n \times n$ slip system interaction matrices (dimensionless units) to be obtained from experimental measurements of self- and latent hardening (cf. [96]), β_{GN} is the length parameter for normalization,

$$\bar{S}^j_{\mathrm{GN}} \equiv |\langle\bar{\mathbf{s}}^j, \bar{\mathbf{S}}^{\mathrm{GN}} \cdot \bar{\mathbf{m}}^j\rangle| \tag{86}$$

is the scalar magnitude of the projected lattice couple stress associated with the GND tensor on slip system j (with the dot product here denoting a contraction of indices on the cotangent space of $\bar{b}_{\mathrm{p}}$), and $\bar{S}^j_{\mathrm{SS}}$ is the lattice stress associated with the SSDs on slip system j. The strain measures of SSDs, $\bar{\varepsilon}^i_{\mathrm{SS}}$, are defined by an additive decomposition of the statistically stored line densities on each slip system, $\bar{\rho}^i_{\mathrm{SS}}$:

$$\bar{\rho}_{\mathrm{SS}} = \sum_{i=1}^{n}\bar{\rho}^i_{\mathrm{SS}} \Rightarrow \bar{\varepsilon}_{\mathrm{SS}} \equiv \tilde{b}\sqrt{\bar{\rho}_{\mathrm{SS}}} = \tilde{b}\sqrt{\sum_{i=1}^{n}\bar{\rho}^i_{\mathrm{SS}}} \equiv \sqrt{\sum_{i=1}^{n}(\bar{\varepsilon}^i_{\mathrm{SS}})^2} \Rightarrow \bar{\varepsilon}^i_{\mathrm{SS}} = \tilde{b}\sqrt{\bar{\rho}^i_{\mathrm{SS}}}. \tag{87}$$

The corresponding thermodynamic force is then, from $(58)_4$, (84), and (87),

$$\bar{S}^i_{\mathrm{SS}} \equiv \frac{\partial\widetilde{\psi}}{\partial\bar{\varepsilon}^i_{\mathrm{SS}}} = \frac{\partial\widetilde{\psi}}{\partial\bar{\varepsilon}_{\mathrm{SS}}}\frac{\partial\bar{\varepsilon}_{\mathrm{SS}}}{\partial\bar{\varepsilon}^i_{\mathrm{SS}}} = \underbrace{\frac{\partial\widetilde{\psi}}{\partial\tilde{\varepsilon}_{\mathrm{SS}}}}_{c_3\mu\tilde{\varepsilon}_{\mathrm{SS}}}\underbrace{\frac{\partial\tilde{\varepsilon}_{\mathrm{SS}}}{\partial\bar{\varepsilon}_{\mathrm{SS}}}}_{\sqrt[-1]{J^{\mathrm{i}}}}\left(\frac{\bar{\varepsilon}^i_{\mathrm{SS}}}{\bar{\varepsilon}_{\mathrm{SS}}}\right) = c_3\mu\sqrt[-1]{J^{\mathrm{i}}}\tilde{\varepsilon}^i_{\mathrm{SS}} = c_3\mu J^{\mathrm{i}-1}\bar{\varepsilon}^i_{\mathrm{SS}}, \tag{88}$$

providing a hardening contribution in (85) proportional to the square root of the dislocation line density per unit volume, as originally suggested by Taylor [97] and since verified experimentally numerous times (cf. [56,98]), and used in both local crystal plasticity theories (cf. [99,100]) and gradient-based theories [34,39,37]. The GND (scalar) couple stresses $\bar{S}^{\mathrm{i}}_{\mathrm{GN}}$ are found explicitly in terms of the tensorial density of GNDs by inserting $(58)_3$ into (86):

$$\bar{S}^{i}_{\mathrm{GN}} = \left| \bar{s}^{i\bar{\alpha}} J^{\mathrm{i}-1} \widetilde{F}^{\mathrm{i}^*\cdot\alpha}_{\bar{\alpha}} \frac{\partial \widetilde{\psi}}{\partial \widetilde{A}^{\mathrm{e}\alpha\beta}} \widetilde{F}^{\mathrm{i}\beta}_{\cdot\bar{\beta}} \bar{g}^{\bar{\beta}\bar{\chi}} \bar{m}^{i}_{\bar{\chi}} \right| = \beta_{\mathrm{GN}} \mu J^{\mathrm{i}-1} \underbrace{\left| \bar{s}^{i\bar{\alpha}} \widetilde{F}^{\mathrm{i}^*\cdot\alpha}_{\bar{\alpha}} \widetilde{A}^{\mathrm{e}}_{\beta\alpha} \widetilde{F}^{\mathrm{i}\beta}_{\cdot\bar{\beta}} \bar{g}^{\bar{\beta}\bar{\chi}} \bar{m}^{i}_{\bar{\chi}} \right|}_{\equiv \bar{A}^{i}_{\mathrm{GN}}} = \beta_{\mathrm{GN}} \mu J^{\mathrm{i}-1} \bar{A}^{i}_{\mathrm{GN}} \tag{89}$$

with $\bar{A}^{i}_{\mathrm{GN}}$ a scalar measure of GNDs on slip system i. Substituting Eqs. (88) and (89) into Eq. (85) then gives

$$\bar{\kappa}^{i} = \bar{\kappa}^{i}_{0} + \mu J^{\mathrm{i}-1} \left(\sqrt{\beta_{\mathrm{GN}}} h^{i}_{\mathrm{GN}j} \bar{A}^{j}_{\mathrm{GN}} + c_3 h^{i}_{\mathrm{SS}j} \bar{\varepsilon}^{j}_{\mathrm{SS}} \right). \tag{90}$$

The contribution of GNDs to individual glide system resistances was previously suggested by Acharya and Bassani [33,73], Acharya and Beaudoin [101], and Bassani [74], for rate-dependent and/or rate-independent single crystal plasticity, similarly to the second term in our Eq. (90).

Many have used the conjugate stress to a tensorial GND measure as a contribution to a *backstress* on each slip system, rather than a contribution to slip system resistance $\bar{\kappa}^{i}$ as in our Eq. (90), with a variety of different ways proposed for projecting the tensorial backstress onto individual glide systems [9,28,32,34,36,37,101]. If both a backstress and a glide stress are desirable in order to completely characterize the hardening behavior (cf. [102]), then we can generalize the flow rule in Eq. (80) to

$$\dot{\gamma}^{i} = \dot{\lambda} \mathrm{sgn}(\bar{p}^{i} - \bar{\chi}^{i}) \left| \frac{\bar{p}^{i} - \bar{\chi}^{i}}{\bar{\kappa}^{i}} \right|^{m}, \tag{91}$$

where increases in the friction stress $\bar{\kappa}^{i} > 0$ now manifest only from SSDs:

$$\bar{\kappa}^{i} = \bar{\kappa}^{i}_{0} + (c_3 \mu J^{\mathrm{i}-1}) h^{i}_{\mathrm{SS}j} \bar{\varepsilon}^{j}_{\mathrm{SS}}, \tag{92}$$

and where the backstress $\bar{\chi}^{i}$, not necessarily positive in sign, depends solely upon the density of GNDs (cf. [34]):

$$\bar{\chi}^{i} = (\mu J^{\mathrm{i}-1} \sqrt{\beta_{\mathrm{GN}}}) h^{i}_{\mathrm{GN}j} \bar{A}^{j}_{\mathrm{GN}}. \tag{93}$$

In Eqs. (92) and (93), $h^{i}_{\mathrm{SS}j}$ and $h^{i}_{\mathrm{GN}j}$ are slip system interaction matrices, different in value, but not in function, from those introduced already in (85). Different, and perhaps more inclusive, ways of expressing the contributions of $\bar{\mathbf{S}}^{\mathrm{GN}}$ to hardening on each slip system than the direct projection method of Eq. (86) also merit further exploration (see e.g. [28,35,36]).

While the density of geometrically necessary dislocations can be calculated directly from spatial gradients of the elastic lattice deformation (Eq. (49)), the densities of statistically stored

dislocations on each slip system are modeled here as internal state variables (ISVs) equipped with separate equations dictating their evolution. By definition, the time rate of change in dislocation density for a given slip system, $\dot{\bar{\rho}}^i_{\mathrm{SS}}$, and the rate of the corresponding dimensionless lattice strain measure $\dot{\bar{\varepsilon}}^i_{\mathrm{SS}}$ for that slip system are related by

$$2\dot{\bar{\varepsilon}}^i_{\mathrm{SS}} = \left(\tilde{b}\sqrt[-1]{\bar{\rho}^i_{\mathrm{SS}}}\right)\dot{\bar{\rho}}^i_{\mathrm{SS}}. \tag{94}$$

A general evolution equation for each dislocation density $\bar{\rho}^i_{\mathrm{SS}}$ is now suggested:

$$\dot{\bar{\rho}}^i_{\mathrm{SS}} = \dot{\bar{\rho}}^i_{\mathrm{SS}}(\{\bar{S}^j_{\mathrm{SS}}\},\{\bar{S}^j_{\mathrm{GN}}\},\{\bar{p}^j\},\bar{\mathbf{S}}^{\mathrm{i}}) \quad (j=1,\ldots,n). \tag{95}$$

As is clear from (95), the dislocation density rate on a particular system i generally includes contributions from the slip rate on the j-th system, via the $\bar{p}^{i=j}$ dependence, as well as the contributions of the slip rates of other systems, through the $\bar{p}^{i\neq j}$ dependence. Likewise, the rate of $\bar{\rho}^i_{\mathrm{SS}}$ may be influenced by the current statistically stored densities on all slip systems through the $\{\bar{S}^j_{\mathrm{SS}}\}$ dependency [80,91]. Since interactions between SSDs and GNDs are not ruled out (e.g., trapping or annihilation), we also allow the densities of GNDs on all slip systems to enter the evolution law for a given system, through the $\{\bar{S}^j_{\mathrm{GN}}\}$ dependency. Finally, the dependency of $\dot{\bar{\rho}}^i_{\mathrm{SS}}$ on $\bar{\mathbf{S}}^{\mathrm{i}} \equiv \widetilde{\mathbf{F}}^{\mathrm{i}-1}\widetilde{\mathbf{S}}^{\mathrm{i}}\widetilde{\mathbf{F}}^{\mathrm{i}-\mathrm{T}}$, the pull-back to $\bar{b}_{\mathrm{p}}$ of the force conjugate to the stretch associated with microscopic heterogeneity within the volume element, is included since the formation of intragranular cellular structures will likely spur dislocation generation and annihilation at misoriented subgrain boundaries [60]. Notice also that $\widetilde{\mathbf{F}}^{\mathrm{i}}$ will implicitly affect the density of GNDs through its presence in the multiplicative decomposition of the total deformation gradient, Eq. (48). More specific rate equations for the SSDs, with dislocation populations further divided into mobile and immobile parts [4,99,100] and accounting for hardening and recovery on each system at different stages of plastic deformation (cf. [34,39]) are also envisioned as possible implementations of (95).

With the evolution of $\overline{\mathbf{F}}^{\mathrm{p}}$ and the strain hardening prescribed by Eqs. (74)–(95), we now turn our attention to the evolution of the $\widetilde{\mathbf{F}}^{\mathrm{i}}$ tensor. The following general evolution equation, referred to configuration $\tilde{b}_{\mathrm{int}}$, is now proposed for the rate of stretching attributed to $\widetilde{\mathbf{F}}^{\mathrm{i}}$:

$$\dot{\widetilde{\mathbf{V}}}^{\mathrm{i}} = \dot{\widetilde{\mathbf{V}}}^{\mathrm{i}}(\widetilde{\mathbf{P}},\widetilde{\mathbf{S}}^{\mathrm{i}},\widetilde{\mathbf{S}}^{\mathrm{GN}},\widetilde{S}^{\mathrm{SS}}), \tag{96}$$

and a similar dependency is proposed for the rate of rotation arising from $\widetilde{\mathbf{F}}^{\mathrm{i}}$, i.e.,

$$\widetilde{\mathbf{W}}^{\mathrm{i}} \equiv \dot{\widetilde{\mathbf{R}}}^{\mathrm{i}}\widetilde{\mathbf{R}}^{\mathrm{iT}} = \widetilde{\mathbf{W}}^{\mathrm{i}}(\widetilde{\mathbf{P}},\widetilde{\mathbf{S}}^{\mathrm{i}},\widetilde{\mathbf{S}}^{\mathrm{GN}},\widetilde{S}^{\mathrm{SS}}). \tag{97}$$

More specific forms of (96) and (97) have not yet been developed. However, previous computational micromechanical solutions indicate that the magnitude of $\widetilde{\mathbf{V}}^{\mathrm{i}}$ should remain small in comparison to the magnitudes of both the total applied strain and the volume-averaged plastic strain in deforming ductile FCC single crystals [88]. The normalized stretch associated with $\widetilde{\mathbf{V}}^{\mathrm{i}}$ was non-negligible, however, and did attain a magnitude comparable to that of the recoverable elastic strain $\widetilde{\mathbf{C}}^{\mathrm{e}}$ in these calculations, as shown in Fig. 6(b). Guidance in formulating Eq. (96) can also stem from the contribution of $\widetilde{\mathbf{V}}^{\mathrm{i}}$ to the stored energy of cold work, as demonstrated in the data of

Fig. 6(a) and suggested in the Helmholtz free energy function (68). We also must note that the calculations used to generate data for Fig. 6 employed local crystal plasticity theory within subgrains, so the influence of GNDs as defined in the present work was neglected in that study [88].

While we currently lack any specific data for the evolution of the rotation tensor $\widetilde{\mathbf{R}}^{\mathrm{i}}$, additional motivation for its inclusion in our crystal plasticity model is acquired by considering the decomposition of the total vorticity in the intermediate configuration $\tilde{b}_{\mathrm{int}}$:

$$(\widetilde{\mathbf{L}})_{\mathrm{skew}} \equiv \widetilde{\mathbf{W}} = \underbrace{(\mathbf{R}^{\mathrm{e}\mathrm{T}}\dot{\mathbf{R}}^{\mathrm{e}})_{\mathrm{skew}}}_{\equiv\widetilde{\mathbf{W}}^{\mathrm{e}}} + (\mathbf{R}^{\mathrm{e}\mathrm{T}}\mathbf{V}^{\mathrm{e}-1}\dot{\mathbf{V}}^{\mathrm{e}}\mathbf{R}^{\mathrm{e}})_{\mathrm{skew}} + (\dot{\widetilde{\mathbf{V}}}^{\mathrm{i}}\widetilde{\mathbf{V}}^{\mathrm{i}-1})_{\mathrm{skew}} + \underbrace{(\widetilde{\mathbf{V}}^{\mathrm{i}}\dot{\widetilde{\mathbf{R}}}^{\mathrm{i}}\widetilde{\mathbf{R}}^{\mathrm{i}\mathrm{T}}\widetilde{\mathbf{V}}^{\mathrm{i}-1})_{\mathrm{skew}}}_{=(\widetilde{\mathbf{V}}^{\mathrm{i}}\widetilde{\mathbf{W}}^{\mathrm{i}}\widetilde{\mathbf{V}}^{\mathrm{i}-1})_{\mathrm{skew}}} + \widetilde{\mathbf{W}}^{\mathrm{p}}, \tag{98}$$

where all skew-symmetrization is conducted with respect to the metric $\tilde{\mathbf{g}}$. Assume for the moment that plastic spin $\widetilde{\mathbf{W}}^{\mathrm{p}}$, spin due to residual stretching rate $\widetilde{\mathbf{V}}^{\mathrm{i}}$, and total spin $\widetilde{\mathbf{W}}$ are prescribed, respectively, via the evolution equations for crystalline slip (Eqs. (74) and (80) or (91)), the evolution equation for strain due to subdivision/heterogeneity (Eq. (96)), and the displacement boundary conditions. Furthermore, assume that second term on the right-hand side of Eq. (98), the elastic spin due to $\dot{\mathbf{V}}^{\mathrm{e}}$, which is known through an appropriate rate form of the constitutive relationship (63) between the applied stress and elastic strain, is negligible in comparison to the other terms in (98) by the typical assumption of small elastic strains in engineering metals. As mentioned previously, since $\widetilde{\mathbf{V}}^{\mathrm{i}}$ is expected to not exceed the same order of magnitude reached by $\mathbf{V}^{\mathrm{e}}$, neglecting the third term in (98) may also be a valid assumption. Under these assumptions, the skew elastic spin $\widetilde{\mathbf{W}}^{\mathrm{e}}$ is then found as

$$\widetilde{\mathbf{W}}^{\mathrm{e}} \approx \widetilde{\mathbf{W}} - \widetilde{\mathbf{W}}^{\mathrm{p}} - (\widetilde{\mathbf{V}}^{\mathrm{i}}\widetilde{\mathbf{W}}^{\mathrm{i}}\widetilde{\mathbf{V}}^{\mathrm{i}-1})_{\mathrm{skew}}. \tag{99}$$

Recall that $\mathbf{F}^{\mathrm{e}}$ provides the current configuration orientations of the "average" slip plane normals and slip directions in our crystal plasticity framework by virtue of Eq. (75); i.e., texture evolution is essentially specified by the time rate of $\mathbf{F}^{\mathrm{e}}$ (cf. [103]). With the assumption of small recoverable elastic strains, we have $\mathbf{F}^{\mathrm{e}} \approx \mathbf{R}^{\mathrm{e}}$, and the time rate of elastic rotation dictates texture evolution. Essentially, we are at liberty to completely control texture evolution through prescription of $\widetilde{\mathbf{W}}^{\mathrm{i}}$, which in turn can be thought of as the contribution to the total spin from intragranular dislocation substructure formation (e.g., grain subdivision processes). For example, if we specify $\widetilde{\mathbf{W}}^{\mathrm{i}} = (\widetilde{\mathbf{V}}^{\mathrm{i}-1}(\widetilde{\mathbf{W}} - \widetilde{\mathbf{W}}^{\mathrm{p}})\widetilde{\mathbf{V}}^{\mathrm{i}})_{\mathrm{skew}}$, then texture evolution (i.e., elastic spin) will be largely precluded due to substructure development within the crystalline volume element. On the other hand if we set $\widetilde{\mathbf{W}}^{\mathrm{i}} = \mathbf{0}$ for our evolution law (97), then crystal lattice orientations will evolve as in the classical crystal plasticity theory. Numerical simulations [50,104] have shown that the classical theory, with $\widetilde{\mathbf{W}}^{\mathrm{i}} = \mathbf{0}$, gives texture predictions that are consistently too-sharp for certain FCC polycrystals, at least within the framework of Taylor's [105] constraints. So by correlating potential evolution Eqs. (97) with experimental texture measurements, one could conceivably formulate evolution laws for $\widetilde{\mathbf{W}}^{\mathrm{i}}$, as speculated by Butler and McDowell [50]. Since grain subdivision and substructure development are energetically favorable, and hence expected, for some materials even under application of macroscopically uniform boundary conditions [7,43,98] $\widetilde{\mathbf{V}}^{\mathrm{i}}$ and/or $\widetilde{\mathbf{W}}^{\mathrm{i}}$ should attain

non-zero values during some point in the history of uniform deformation applied to such materials.

In closing the discussion of evolution equations, we emphasize that when completely developing Eqs. (95)–(97), which we have left quite general in this work, one should also consider the restrictions on thermodynamic admissibility stemming from the complete dissipation inequality, Eq. (67). While we have included terms associated with dislocation defect densities and residual elasticity in the free energy function (68), in most metals their total cumulative contribution to the first and second laws of thermodynamics, (54) and (55), will remain relatively small in magnitude compared to that of the plastic dissipation due to dislocation motion (77), in agreement with experimental measurements of the stored energy of cold working [106,107]. This observation is fully consistent with the framework presented here (cf. Eq. (68)); the contribution of incompatibility- related tensors (i.e., $\widetilde{\mathbf{F}}^{\mathrm{i}}$ and defect densities) to the free energy is small when averaged over the entire volume of the crystal(s). The relatively small magnitude of this energetic contribution is scaled correctly by the appropriate choice of material parameters in (68). However, in our opinion, the residual elastic energy associated with crystal defects and elastoplastic incompatibility should not be neglected, as its local density may attain much greater magnitudes in the vicinity of local heterogeneities such as grain or phase boundaries, and its release may facilitate void growth, fracture, shear localization, recrystallization, and/or phase transition processes in many metals [88,108].

5. Conclusions

We have used explicit volume averaging procedures (Sections 2 and 3) to motivate a continuum formulation of gradient crystal plasticity (Section 4). Notable features include

- A three-term multiplicative decomposition for the deformation gradient, $\mathbf{F} = \mathbf{F}^{\mathrm{e}}\widetilde{\mathbf{F}}^{\mathrm{i}}\overline{\mathbf{F}}^{\mathrm{p}}$, with $\mathbf{F}^{\mathrm{e}}$ associated with the average applied stress and total lattice rotation, $\widetilde{\mathbf{F}}^{\mathrm{i}}$ accounting for the possible development of heterogeneous dislocation substructures and residual elasticity, and $\overline{\mathbf{F}}^{\mathrm{p}}$ accounting for the history of plastic deformation due to dislocation motion.
- Prescription of a resolved Eshelby-type stress measure as a driving force for plastic shearing rates, in order to ensure a positive dissipation contribution from the plastic velocity gradient.
- Slip system-level strain hardening dependent upon conjugate thermodynamic forces to densities of GNDs and SSDs.
- Allowance of $\widetilde{\mathbf{F}}^{\mathrm{i}}$, the kinematic measure of intragranular heterogeneity and possible subdivision, to influence the evolution of dislocation densities, and vice-versa.
- Allowance of a measure of residual elasticity—the stretch associated with $\widetilde{\mathbf{F}}^{\mathrm{i}}$—to account for a fraction of the stored energy of cold work, influence the effective elastic moduli in the unloaded configuration, and provide a residual free energy term biased by the applied stress.

Our framework offers powerful tools for addressing multiscale issues in plasticity, most notably providing a very rigorous (i.e., mathematically precise) methodology for characterizing kinematics and thermodynamics with changes in scale of observation. Future work should focus on determination of more precise evolution equations for $\widetilde{\mathbf{F}}^{\mathrm{i}}$ and the dislocation densities, determination

of the needed material parameters (e.g., hardening coefficients and length scale constants), and exploration of boundary conditions. Micromechanical simulations of representative defect populations invoking discrete dislocation dynamics relations [109–111] are foreseen as valuable tools for deducing evolution laws and model parameters. Extensions to other defects (e.g., disclinations, point defects, and damage), temperature effects, and dynamic conditions are also envisioned.

Acknowledgements

J.D.C. and D.L.M. are grateful for the support of the Army Research Office (ARO Award DAAD19-99-1-0221). D.J.B. acknowledges the support of Sandia National Laboratories. Sandia is a multiprogram laboratory operated by Sandia Corporation, a Lockheed Martin Company, for the United States Department of Energy under Contract DE-AC04-94AL85000.

References

[1] C. Teodosiu, Rev. Roum. Sci. Tech.—Méch. Appl. 12 (1967) 961–977.
[2] C. Teodosiu, Rev. Roum. Sci. Tech.—Méch. Appl. 12 (1967) 1291–1308.
[3] C. Teodosiu, A dynamic theory of dislocations and its application to the theory of elastic–plastic continuum, in: Proceedings of the Conference on Fundamental Aspects of Dislocation Theory, Washington, 1969, pp. 837–876.
[4] R.W. Lardner, Z. Agnew Math. Phys. 20 (1969) 514–529.
[5] O.W. Dillon, J. Kratochvil, Int. J. Solids Struct. 6 (1970) 1513–1533.
[6] O.W. Dillon, P. Perzyna, Arch. Mech. 24 (1972) 727–747.
[7] M. Ortiz, E.A. Repetto, J. Mech. Phys. Solids 47 (1999) 397–462.
[8] H.M. Zbib, E.C. Aifantis, Acta Mech. 92 (1992) 209–225.
[9] A. Menzel, P. Steinmann, J. Mech. Phys. Solids 48 (2000) 1777–1796.
[10] D.L. Holt, J. Appl. Phys. 41 (1970) 3197–3201.
[11] D.J. Bammann, E.C. Aifantis, Acta Mech. 45 (1982) 91–121.
[12] E.C. Aifantis, Int. J. Plast. 3 (1987) 211–247.
[13] M.E. Gurtin, J. Mech. Phys. Solids 48 (2000) 989–1036.
[14] A.C. Eringen, J. Appl. Phys. 56 (1984) 2675–2680.
[15] E.C. Aifantis, J. Eng. Mater. Tech. 121 (1999) 189–202.
[16] K. Shizawa, H. Zbib, Int. J. Plast. 15 (1999) 899–938.
[17] K. Shizawa, H. Zbib, J. Eng. Mater. Tech. 121 (1999) 247–253.
[18] E.O. Hall, Phys. Soc. London Proc. 64 (1951) 747–753.
[19] N.J. Petch, J. Iron, Steel Inst. 174 (1953) 25–28.
[20] J.Y. Shu, N.A. Fleck, J. Mech. Phys. Solids 47 (1999) 297–324.
[21] S. Forest, F. Barbe, G. Cailletaud, Int. J. Solids Struct. 37 (2000) 7105–7126.
[22] E. Cosserat, F. Cosserat, C.R. Acad. Sci. Paris 145 (1907) 1139–1142.
[23] E. Cosserat, F. Cosserat, Théorie des Corps Déformables, Hermann, Paris, 1909, p. vi+, 226.
[24] N.A. Fleck, G.M. Muller, M.F. Ashby, J.W. Hutchinson, Acta Metall. Mater. 42 (1994) 475–487.
[25] J.Y. Shu, N.A. Fleck, Int. J. Solids Struct. 35 (1998) 1363–1383.
[26] K.C. Hwang, H. Jiang, Y. Huang, H. Gao, N. Hu, J. Mech. Phys. Solids 50 (2002) 81–99.
[27] N.A. Fleck, J.W. Hutchinson, J. Mech. Phys. Solids 41 (1993) 1825–1857.
[28] P.M. Nagdhi, A.R. Srinivasa, Int. J. Eng. Sci. 32 (1994) 1157–1182.
[29] K.C. Le, H. Stumpf, Proc. R. Soc. London A 452 (1996) 359–371.
[30] K.C. Le, H. Stumpf, Int. J. Plast. 12 (1996) 611–627.
[31] K.C. Le, H. Stumpf, Int. J. Eng. Sci. 34 (1996) 339–358.

[32] P. Steinmann, Int. J. Eng. Sci. 34 (1996) 1717–1735.
[33] A. Acharya, J.L. Bassani, J. Mech. Phys. Solids 48 (2000) 1565–1595.
[34] D.J. Bammann, Mater. Sci. Eng. A 309–310 (2001) 406–410.
[35] P. Cermelli, M.E. Gurtin, J. Mech. Phys. Solids 49 (2001) 1539–1568.
[36] M.E. Gurtin, J. Mech. Phys. Solids 50 (2002) 5–32.
[37] B. Svendsen, J. Mech. Phys. Solids 50 (2002) 1297–1329.
[38] P.M. Nagdhi, A.R. Srinivasa, Philos. Trans. R. Soc. London A 345 (1993) 425–458.
[39] R.A. Regueiro, D.J. Bammann, E.B. Marin, K. Garikipati, J. Eng. Mater. Technol. 124 (2002) 380–387.
[40] M.F. Ashby, Philos. Mag. 21 (1970) 399–424.
[41] D. Kuhlmann-Wilsdorf, N. Hansen, Scr. Met. Mater. 25 (1991) 1557–1562.
[42] B. Bay, N. Hansen, D.A. Hughes, D. Kuhlmann-Wilsdorf, Acta Metall. Mater. 40 (1992) 205–219.
[43] D.A. Hughes, Q. Liu, D.C. Chrzan, N. Hansen, Acta Mater. 45 (1997) 105–112.
[44] D. Kuhlmann-Wilsdorf, Philos. Mag. A 79 (1999) 955–1008.
[45] G.C. Butler, S.R. Stock, D.L. McDowell, Key Eng. Mater. 177–180 (2000) 165–170.
[46] N.R. Barton, P.R. Dawson, Metal. Mater. Trans. 32A (2001) 1967–1975.
[47] T. Leffers, Int. J. Plast. 17 (2001) 469–489.
[48] T. Leffers, Mater. Sci. Forum 157–162 (1994) 1815–1820.
[49] T. Leffers, Int. J. Plast. 17 (2001) 491–511.
[50] G.C. Butler, D.L. McDowell, Int. J. Plast. 14 (1998) 703–717.
[51] M.F. Horstemeyer, D.L. McDowell, Mech. Mater. 27 (1998) 145–163.
[52] M.F. Horstemeyer, D.L. McDowell, R.D. McGinty, Mod. Sim. Mater. Sci. Eng. 7 (1999) 253–273.
[53] M. Berveiller, D. Muller, J. Kratochvil, Int. J. Plast. 9 (1993) 633–652.
[54] M. Ortiz, E.A. Repetto, L. Stainier, J. Mech. Phys. Solids 48 (2000) 2077–2114.
[55] D. Hughes, N. Hansen, Mater. Sci. Technol. 7 (1991) 544–553.
[56] D. Kuhlmann-Wilsdorf, Metal. Trans. 16A (1985) 2091–2108.
[57] C. Carstensen, K. Hackl, A. Mielke, Proc. R. Soc. London A 458 (2002) 299–317.
[58] S. Takeuchi, A.S. Argon, J. Mater. Sci. 11 (1976) 1542–1566.
[59] J.C. Gibeling, W.D. Nix, Acta Metall. 28 (1980) 1743–1752.
[60] A.S. Argon, S. Takeuchi, Acta Metall. 29 (1981) 1877–1884.
[61] R. Hill, Proc. R. Soc. London A 326 (1972) 131–147.
[62] J.D. Clayton, B.M. Schroeter, D.L. McDowell, S. Graham, J. Eng. Mater. Technol. 124 (2002) 302–313.
[63] J.A. Schouten, Ricci Calculus, second ed., Springer-Verlag, Berlin, 1954.
[64] K. Kondo, On the geometrical and physical foundations of the theory of yielding, in: Proceedings of the 2nd Japan Congress on Applied Mechanics, Japan National Committee for Theoretical and Applied Mechanics, Science Council of Japan, Tokyo, 1953, pp. 41–47.
[65] B.A. Bilby, R. Bullough, E. Smith, Proc. R. Soc. London A 231 (1955) 263–273.
[66] E. Kröner, Arch. Rat. Mech. Anal. 4 (1960) 273–334.
[67] G.A. Maugin, Material Inhomogeneities in Elasticity, Chapman & Hall, London, 1993.
[68] A. Arsenlis, D.M. Parks, Acta Mater. 47 (1999) 1597–1611.
[69] E. Kröner, Int. J. Solids Struct. 38 (2001) 1115–1134.
[70] B.A. Bilby, E. Smith, Proc. R. Soc. London A 232 (1956) 481–505.
[71] S. Nemat-Nasser, Mech. Mater. 31 (1999) 493–523.
[72] R. Hill, Math. Proc. Camb. Philos. Soc. 95 (1984) 481–494.
[73] A. Acharya, J.L. Bassani, Incompatible lattice deformations and crystal plasticity, in: N. Ghoniem (Ed.), Plastic and Fracture Instabilities in Materials, AMD 200/MD 57, ASME, NY, 1995, pp. 75–80.
[74] J.L. Bassani, J. Mech. Phys. Solids 49 (2001) 1983–1996.
[75] J. Mandel, Thermodynamics and plasticity, in: J.J. Delgado et al. (Eds.), Continuum Thermodynamics, Macmillan, New York, 1974, pp. 283–304.
[76] K.C. Le, H. Schutte, H. Stumpf, Int. J. Plast. 14 (1998) 1109–1131.
[77] J. Kratochvil, Finite-strain theory of inelastic behavior of crystalline solids, in: A. Sawzcuk (Ed.), Foundations of Plasticity, Warsaw, 1972, pp. 401–415.

[78] A. Lion, Int. J. Plast. 16 (2000) 469–494.
[79] E. Kröner, J. Math. Phys. 42 (1963) 27–37.
[80] C. Teodosiu, F. Sidoroff, Int. J. Eng. Sci. 14 (1976) 713–723.
[81] E. Van der Giessen, F.G. Kollmann, Z. Agnew. Math. Mech. 76 (1996) 447–462.
[82] H. Stumpf, U. Hoppe, Z. Agnew Math. Mech. 77 (1997) 327–339.
[83] B.D. Coleman, W. Noll, Arch. Rat. Mech. Anal. 13 (1963) 167–178.
[84] B.D. Coleman, M.E. Gurtin, J. Chem. Phys. 17 (1967) 597–613.
[85] G.A. Maugin, Int. J. Plast. 10 (1994) 393–408.
[86] J.D. Eshelby, J. Elast. 5 (1975) 321–335.
[87] K.-Ch. Le, H. Stumpf, Acta Mech. 100 (1993) 155–170.
[88] J.D. Clayton, D.L. McDowell, Int. J. Plast. 19 (2003) 1401–1444.
[89] J.C. Simo, M. Ortiz, Comp. Meth. Appl. Mech. Eng. 49 (1985) 221–245.
[90] A. Cuitiño, M. Ortiz, Eng. Computat. 9 (1992) 437–452.
[91] J.R. Rice, J. Mech. Phys. Solids 19 (1971) 433–455.
[92] R. Hill, K.S. Havner, J. Mech. Phys. Solids 30 (1982) 5–22.
[93] R.J. Asaro, J. Appl. Mech. 50 (1983) 921–934.
[94] J.W. Hutchinson, Proc. R. Soc. London A 348 (1976) 101–127.
[95] E. Schmid, in: Proceedings of the International Congress of Applied Mechanics, Delft, 1924, p. 342.
[96] U.F. Kocks, Metall. Trans. 1 (1970) 1121–1143.
[97] G.I. Taylor, Proc. R. Soc. London A 145 (1934) 362–415.
[98] D. Kuhlmann-Wilsdorf, Mater. Sci. Eng. A 113 (1989) 1–41.
[99] M.A. Zikry, M. Kao, J. Mech. Phys. Solids 44 (1996) 1765–1798.
[100] T. Kameda, M.A. Zikry, Scr. Mater. 38 (1998) 631–636.
[101] A. Acharya, A.J. Beaudoin, J. Mech. Phys. Solids 48 (2000) 2213–2230.
[102] D.L. McDowell, J.C. Moosbrugger, Acta Mech. 93 (1992) 73–87.
[103] R.J. Asaro, A. Needleman, Acta Metall. 33 (1985) 923–953.
[104] U.F. Kocks, M.G. Stout, A.D. Rollett, The influence of texture on strain hardening, in: Strength of Metals and Alloys, vol. 1, 1988, pp. 25–34.
[105] G.I. Taylor, J. Inst. Metals 62 (1938) 307.
[106] G.I. Taylor, H. Quinney, Proc. R. Soc. London A 143 (1934) 307–326.
[107] P. Rosakis, A.J. Rosakis, G. Ravichandran, J. Hodowany, J. Mech. Phys. Solids 48 (2000) 581–607.
[108] S.P.A. Gill, M.G. Cornforth, A.C.F. Cocks, Int. J. Plast. 17 (2001) 669–690.
[109] H.M. Zbib, M. Rhee, J.P. Hirth, Int. J. Mech. Sci. 40 (1998) 112–127.
[110] J.L. Bassani, A. Needleman, E. Van der Giessen, Int. J. Solids Struct. 38 (2000) 833–853.
[111] A. Needleman, Acta Mater. 48 (2000) 105–124.

NO. OF
COPIES ORGANIZATION

1 (PDF ONLY) DEFENSE TECHNICAL INFORMATION CTR
DTIC OCA
8725 JOHN J KINGMAN RD
STE 0944
FORT BELVOIR VA 22060-6218

1 US ARMY RSRCH DEV & ENGRG CMD
SYSTEMS OF SYSTEMS INTEGRATION
AMSRD SS T
6000 6TH ST STE 100
FORT BELVOIR VA 22060-5608

1 INST FOR ADVNCD TCHNLGY
THE UNIV OF TEXAS
AT AUSTIN
3925 W BRAKER LN
AUSTIN TX 78759-5316

1 DIRECTOR
US ARMY RESEARCH LAB
IMNE ALC IMS
2800 POWDER MILL RD
ADELPHI MD 20783-1197

3 DIRECTOR
US ARMY RESEARCH LAB
AMSRD ARL CI OK TL
2800 POWDER MILL RD
ADELPHI MD 20783-1197

ABERDEEN PROVING GROUND

1 DIR USARL
AMSRD ARL CI OK TP (BLDG 4600)

NO. OF
COPIES ORGANIZATION

ABERDEEN PROVING GROUND

30 DIR USARL
AMSRD ARL CI HC
P CHUNG
C CORNWELL
AMSRD ARL WM
M FERMEN COKER
T WRIGHT
J MCCAULEY
AMSRD ARL WM MA
W NOTHWANG
AMSRD ARL WM TA
S SCHOENFELD
AMSRD ARL WM TD
S BILYK
T BJERKE
D CASEM
J CLAYTON (10 CPS)
D DANDEKAR
M GREENFIELD
Y HUANG
K IYER
B LOVE
M RAFTENBERG
E RAPACKI
M SCHEIDLER
S SEGLETES
T WEERASOORIYA

INTENTIONALLY LEFT BLANK.